SPATIO-TEMPORAL MONITORING OF SURFACE DEFORMATION ON THE NORTH ANATOLIAN FAULT ZONE

by

Çağkan Serhun Zoroğlu

B.S., Geophysical Engineering, Istanbul Technical University, 2021

Submitted to the Kandilli Observatory and Earthquake
Research Institute in partial fulfillment of
the requirements for the degree of
Master of Science

Graduate Program in Geodesy

Boğaziçi University

2024

SPATIO-TEMPORAL MONITORING OF SURFACE DEFORMATION ON THE NORTH ANATOLIAN FAULT ZONE

APPROVED BY:

Assist. Prof. Tülay Kaya Eken ..... (Thesis Supervisor)

Prof. Dr. Haluk Özener .....

Assoc. Prof. Muharrem Hilmi Erkoç .....

DATE OF APPROVAL: 24.07.2024

ACKNOWLEDGEMENTS

First of all, I would like to thank my supervisor Assist. Prof. Tülay Kaya Eken for her endless support and for her advices not only about academia but also about life. She always motivated me when I needed the most and she also encouraged me to research the topics I was curious about. She helped me start asking the right questions in terms of earth sciences and spent hours reading articles with me to improve my research techniques and theoretical knowledge. She always gave me time and space when I wasn't feeling well and didn't pressure me into what I needed to do. And I think most importantly, no matter what the circumstances, she always kept a smile on her face for me.

I would also like to express my deep gratitude to my undergraduate thesis teacher, Associate Professor Tuna Eken. During my undergraduate studies, even though I met him very late during my undergraduate studies, I would like to thank him for never leaving me alone or without support, for seeing the same love for science in me as he did, and for always trying to teach something new to me.

I would like to express my deep gratitude to Prof. Dr. Haluk Özener, who made every effort to ensure that I did not feel like a stranger since I first came to Boğaziçi University Kandilli Observatory and Earthquake Research Center, who provided all kinds of help so that I could learn what I was curious about and progress in earth sciences, and who encouraged me to take responsibility and trusted me. In my eyes, he represents the culture of Boğaziçi University Kandilli Observatory and Earthquake Research Center.

I would also like to thank Mehmet Buğrahan Atar for constantly contributing to my self-improvement, for always being there for me, for helping me whenever I was in trouble, making fun plans with me, and most importantly, for the unrequited friendship he gave me.

I would also like to thank Berkay Kan for always being there for me, for helping me whenever I was in trouble, for being a friend with whom I could share everything, and for helping me improve myself in computers and software.

I would like to thank Merve Ercan, Mısra Gedik and Gülşen Tekiroğlu for always being there for me, for always being ready to take on the workload so that I would not have to shoulder it, and for the help they gave me whenever I needed it.

I would like to thank Barış Can Köse for always being there for me, for helping me whenever I got stuck, and for never missing a moment of fun and smile from even his friends' lives.

Finally, I would like to thank my beloved mother, Emine Gürsel Zoroğlu, my beloved father, Bahri Zoroğlu, and my beloved sister, Beliz Selen Zoroğlu for giving me the opportunity to do whatever I want at every moment of my life, for never missing their support for a moment, for facing those difficulties more than me whenever I had difficulties, for the unconditional love and support they gave me. Sizi çok seviyorum.

ABSTRACT

SPATIO-TEMPORAL MONITORING OF SURFACE DEFORMATION ON THE NORTH ANATOLIAN FAULT ZONE

The North Anatolian Fault Zone (NAFZ) is a major transform boundary between the Anatolian and Eurasian plates, this right-lateral strike slip fault system generated devastating seismic events during the 20th century. In this thesis, we applied Interferometric Synthetic Aperture Radar (InSAR) time series analysis, utilizing Sentinel-1 data from the period 2014 to 2022, with the objective of analyzing surface deformation and the relationship between crustal properties and fault mechanics in the Düzce section of the NAFZ. Analysis of Sentinel-1 data using the Small Baseline Subset technique reveals deformation patterns on the Düzce Fault, indicating a slip rate of approximately 2.5 - 3 cm/yr. In addition to the long term deformation analysis in the Duzce region, this thesis investigates the impacts of the 2022 Mw6.0 Gölyaka-Düzce earthquake by comparing pre- and post-seismic deformation using ascending and descending InSAR datasets. The thesis integrates geophysical data obtained from magnetotelluric surveys and seismic tomography, offering valuable information about subsurface features such as fluid-saturated and fractured rock zones. This integration emphasizes the crucial areas of roughness and the buildup of significant strain, which are vital for comprehending seismic risks. The results of our study highlight the importance of continuous monitoring and the integration of geophysical techniques to enhance earthquake preparedness and reduce the risks in the Düzce region. This technique improves our understanding of the complex geodynamic processes occurring along the NAFZ.

ÖZET

KUZEY ANADOLU FAY ZONUNDA YÜZEY DEFORMASYONUNUN UZAY-ZAMANLI İZLENMESİ

Kuzey Anadolu Fay Zonu (KAFZ), Anadolu ve Avrasya plakaları arasındaki önemli bir transform sınırdır. Bu sağ-yanal doğrultu-atımlı fay sistemi 20. yüzyıl boyunca yıkıcı sismik olaylara neden olmuştur. Bu tezde, KAFZ'nin Düzce kesiminde yüzey deformasyonunu ve kabuk özellikleri ile fay mekaniği arasındaki ilişkiyi analiz etmek amacıyla 2014-2022 dönemine ait Sentinel-1 verilerini kullanarak İnterferometrik Sentetik Açıklıklı Radar (InSAR) zaman serisi analizi uyguladık. Sentinel-1 gözlemleri, Small Baseline Subset (SBAS) yöntemiyle analiz edilerek Düzce Fayı'nda $\sim 2.5 - 3$ cm/yr kayma oranıyla deformasyon modellerini ortaya koymaktadır. Düzce bölgesindeki uzun vadeli deformasyon analizine ek olarak, bu tez, hem yükselen yörüngeli hem de alçalan yörüngeli InSAR veri setlerini kullanarak 2022 Mw6.0 Gölyaka-Düzce depreminin öncesi ve sonrası yüzey deformasyonunu karşılaştırmaktadır. Bu tez, bölgede daha önce yapılmış manyetotellürik (MT) araştırmalar ve sismik tomografiden elde edilen jeofizik verileri de içermekte olup, sıvı doygun ve çatlaklı kaya zonları gibi yer altı özellikleri hakkında bilgi sağlamaktadır. Bu entegrasyon, yüksek gerilme birikimi ve asperit zonları gibi kritik alanları vurgulayarak, sismik tehlikeleri anlamak için önemlidir. Bulgularımız, Düzce bölgesinde deprem hazırlığı ve risk azaltma stratejilerini iyileştirmek için sürekli izleme ve çeşitli jeofizik yöntemlerin entegrasyonunun önemini vurgulamaktadır. Bu yaklaşım, KAFZ boyunca karmaşık jeodinamik süreçlerin anlaşılmasını kolaylaştırmaktadır.

TABLE OF CONTENTS

ACKNOWLEDGEMENTS iii
ABSTRACT v
ÖZET vi
LIST OF FIGURES ix
LIST OF TABLES xiv
LIST OF SYMBOLS xv
LIST OF ACRONYMS/ABBREVIATIONS xvi
1. INTRODUCTION 1
2. STUDY REGION 5
2.1. Tectonic Setting of Türkiye and the NAFZ 5
2.2. Geology and Tectonics of the Düzce Region 8
2.3. Previous Studies in Düzce Region 9
2.3.1. Geodetic Studies 9
2.3.2. Geophysical Studies 13
3. METHODOLOGY 18
3.1. Geodetic Methods 18
3.1.1. Interferometric Synthetic Aperture Radar (InSAR) 18
3.1.2. Processing Steps for InSAR 22
3.1.3. Time Series Analysis 26
3.2. Geophysical Methods 28
3.2.1. Coulomb Stress Analysis 28
4. DATA & DATA PROCESS 30
4.1. Data Acquisition 30
4.2. Interferogram Generation & Stack 31
4.3. Velocity Calculation with SBAS 33
5. Results 34
5.1. InSAR Time Series Analysis 34

5.2. InSAR Co-seismic Analysis of 23 November 2022 Mw6.0 Gölyaka (Düzce) Earthquake 38
5.3. Coulomb Stress Analysis of 23 November 2022 Mw6.0 Gölyaka (Düzce) Earthquake 43
6. Discussion & Conclusion 51
6.1. Comparison with Seismic Tomography and Magnetotelluric Surveys . . 51
6.2. Implications for Seismic Hazard Assessment 52
6.3. Conclusion 53
REFERENCES 55

LIST OF FIGURES

Figure 1.1. Tectonic setting of Türkiye (Wang et al., 2020). Suture zones are shown by the thick black lines (Wang et al., 2020; Okay & Tüysüz, 1999). The late Cenozoic volcanic centers are shown by the red triangles. Major faults and trenches are shown by the red lines. . . 1

Figure 1.2. Historical earthquakes along NAFZ show the earthquake migration to the west (Pınar et al., 2016). Colored segments represent the major earthquakes and fault ruptures that have occurred along the North Anatolian Fault (NAF) since the December 26, 1939, Erzincan earthquake. 2

Figure 1.3. Seismic cycle description with using the elastic rebound model of Reid (1910) (modified from Wright, (2002). 3

Figure 2.1. Tectonic map illustrating the main continental blocks and sutures in the northern Mediterranean region. Filled triangles reveal the polarity of previous subduction zones. Grey tones highlight the Black Sea's Late Cretaceous oceanic crust. Rewritten in light of Şengör (1984) Okay (1989), and Okay et al. (1994, 1996) (Okay & Tüysüz, 1999) 6

Figure 2.2. PS InSAR models on the İzmit and Düzce Region. 11

Figure 2.3. The tectonic setting of Anatolia and the interseismic surface velocities (Weiss et al., 2020), measured in a reference frame that is fixed to Eurasia. The GNSS velocity vectors from England et al. [2016] and Nocquet [2012] demonstrate the counterclockwise rotation of Anatolia and Arabia in relation to Eurasia. 13

Figure 2.4. Models of magnetotelluric profiles on the Düzce Region (Kaya et al., 2009). The black triangles indicates MT stations. The red triangles represent the NAF and the Düzce fault, in that order, from a southern to northern direction. The circles depict areas of aftershocks, with sparse dots representing regions of few aftershocks and dense dots representing regions of many aftershocks. 17

Figure 3.1. Synthetic-aperture radar acquisition representation modified from Anderlini, (2014). 19

Figure 3.2. SAR acquisition modes representation (taken from ESA's website). Stripmap mode, Interferometric WideSwath mode, Extra WideSwath mode and Wave mode are described from left to right. 20

Figure 3.3. Sentinel-1 TOPS Acquisiton Geometry modified from Yu et al. (2019). 21

Figure 3.4. An ERS-2 Synthetic Aperture Radar (SAR) image of Mount Vesuvius in Italy, captured and identified by ESA. The image exhibits a vertical slant range direction, with the near range being in the upper section of the image. Higher degrees of brightness are indicative of more intense backscattered radiation. 23

Figure 3.5. Interferogram example obtained from ascending orbit data. 25

Figure 3.6. Example of an ascending orbit unwrapped interferogram. 26

Figure 3.7. Interferogram stack generation and SBAS-InSAR basic processing workflow obtained from Liu et al. (2023). 27

Figure 5.1. Interferogram network of ascending orbit SLCs used. Continuous line represents the used interferograms and the dashed line represents the extracted interferograms. Data from October 10 2022 to 2023 are excluded. Cold colors represent the high coherence between SLC pairs and warm colors represent the low coherence between SLC pairs. 35

Figure 5.2. Interferogram network of descending orbit SLCs used. Continuous line represents the used interferograms and the dashed line represents the dropped interferograms. Data from 2014 to 02.06.2017 are excluded. Cold colors represent the high coherence between SLC pairs and warm colors represent the low coherence between SLC pairs. 36

Figure 5.3. Geocoded average spatial coherence of ascending data. Bright colors represent high coherence and the dim colors represent low coherence. 36

Figure 5.4. Geocoded temporal coherence of ascending data. Bright colors represent areas of high coherence and dim colors represent areas of low coherence. 37

Figure 5.5. Geocoded average spatial coherence of descending data. Bright colors represent areas of high coherence and dim colors represent areas of low coherence. 38

Figure 5.6. Geocoded temporal coherence of descending data. Bright colors represent areas of high coherence and dim colors represent areas of low coherence. 39

Figure 5.7. Unmasked velocity map obtained from MintPY with using ascending SLCs. Warm colors represent the positive velocities (motion towards the reference point.) and the cold colors represent the negative velocities (motion away from the reference point). 40

Figure 5.8. Unmasked velocity map obtained from MintPY with using descending SLCs. Warm colors represent the positive velocities (motion through the reference point.) and the cold colors represent the negative velocities (motion away from the reference point). 41

Figure 5.9. Adjusted velocity map between -3 cm/ year and 3 cm/year obtained from MintPY with using ascending SLCs. Warm colors represent the positive velocities (motion through the reference point.) and the cold colors represent the negative velocities (motion away from the reference point). 42

Figure 5.10. Adjusted velocity map between -3 cm/ year and 3 cm/year obtained from MintPY with using descending SLCs. Warm colors represent the positive velocities (motion through the reference point.) and the cold colors represent the negative velocities (motion away from the reference point). 43

Figure 5.11. The coherence map of ascending interferogram obtained from ISCE2. Bright colors represent the high coherence and the dim colors represent the low coherence. 44

Figure 5.12. The coherence map of descending interferogram obtained from ISCE2. Bright colors represent the high coherence and the dim colors represent the low coherence. 45

Figure 5.13. Wrapped interferogram obtained by using ascending orbit SLCs. . 46

Figure 5.14. Unwrapped interferogram obtained by using ascending orbit SLCs. Warm colors represent the motion away from the satellite and the cold colors represent the motion towards the satellite. 47

Figure 5.15. Unwrapped masked interferogram masked with coherence file, obtained by using ascending orbit SLCs. Warm colors represent the motion away from the satellite and the cold colors represent the motion towards the satellite. 47

Figure 5.16. Wrapped interferogram obtained by using descending orbit SLCs. 48

Figure 5.17. Unwrapped interferogram obtained by using descending orbit SLCs. Warm colors represent the motion away from the satellite and the cold colors represent the motion towards the satellite. 48

Figure 5.18. Coulomb stress analysis of 23 November 2022 Düzce earthquake. Warm colors represent the stress buildup and the cold colors represent the stress relief. 77° of strike, 65° of dip and −168° of rake is used as fochal mechanism solution parameters (Obtained from AFAD). Depth is 6.81 km and friction coefficient is 0.4. 49

Figure 5.19. Coulomb stress analysis of 23 November 2022 Düzce earthquake with aftershocks. 77 degrees of strike, 65 degrees of dip and -168 degrees of rake is used for the mainshock as focal mechainsm solution parameters (Obtained from AFAD). Depth is fixed to 10 km and friction coefficient is 0.4. 49

Figure 5.20. 77 degrees of strike, 65 degrees of dip and -168 degrees of rake is used as fochal mechainsm solution parameters (Obtained from AFAD. Depth is ranged from 0 to 15 km and friction coefficient is 0.4. 50

LIST OF TABLES

Table 5.1. Earthquake catalog and fault parameters obtained from AFAD . . 45

LIST OF SYMBOLS

$\mathbf{d}$	Vector of observed phase differences
$\mathbf{D}$	Fault slip
E	Elastic modulus
$\mathbf{G}$	Design matrix containing the temporal and spatial baselines
$\mathbf{m}$	Vector of deformation parameters
$\mathbf{n}$	Noise vector
t_i	Time period for each event i
u_i	Observed slip for each event i
$u(x)$	Surface displacement
v	Seismic wave velocity
v_{plate}	Tectonic plate velocity
x	Distance from the fault
Δd	Ground displacement
ΔP	Pore pressure change
Δr	Change in the range distance
$\Delta\sigma_f$	Coulomb failure
$\Delta\sigma_n$	Change in normal stress
Δt_{ij}	Difference in travel time between two earthquakes i and j
$\Delta\tau$	Change in shear stress
$\Delta\phi$	Phase difference
λ	Wavelength of the radar signal
μ	Coefficient of friction
ϕ_i	Phase of ith image
ρ	Density of the material

LIST OF ACRONYMS/ABBREVIATIONS

ATB	Anatolide-Tauride Block
BFZ	The Bornova-Flysch Zone
CAP	Central Anatolian Province
DSFZ	Dead Sea Fault Zone
EACP	East Anatolian Contractional Province
EAFZ	East Anatolian Fault Zone
EAP	East Anatolian Plateau
GPS	Ground Positioning System
IA	Isparta Angle
IAESZ	İzmir-Ankara-Erzincan Suture zone
InSAR	Interferometric Synthetic Aperture Radar
IPSZ	Intra-Pontide Suture Zone
ISCE2	Interferometric synthetic aperture radar Scientific Computing Environment
IZ	İstanbul Zone
KB	Kırşehir Block
MintPY	Miami InSAR Time Series software in Python
NAFZ	North Anatolian Fault Zone
RSZ	Rhodope-Strandja Zone
SAR	Synthetic Aperture Radar
SBAS	Small Baseline Subset
SZ	Sakarya zone
TB	Thrace Basin
WAEP	Western Anatolian Extensional Province

1. INTRODUCTION

Türkiye's tectonic environment is shaped by the relative motions between the Eurasian, Anatolian, African, and Arabian plates, making it one of the most seismically active regions globally. The convergence of these plates results in seismic activities that influence the geological and geophysical features of the region. The Anatolian Plate is subjected to westward displacement due to pressure from the northward-moving the Arabian Plate, leading to significant lateral movement along the North Anatolian Fault Zone (NAFZ) (Şengör & Yılmaz, 1981).

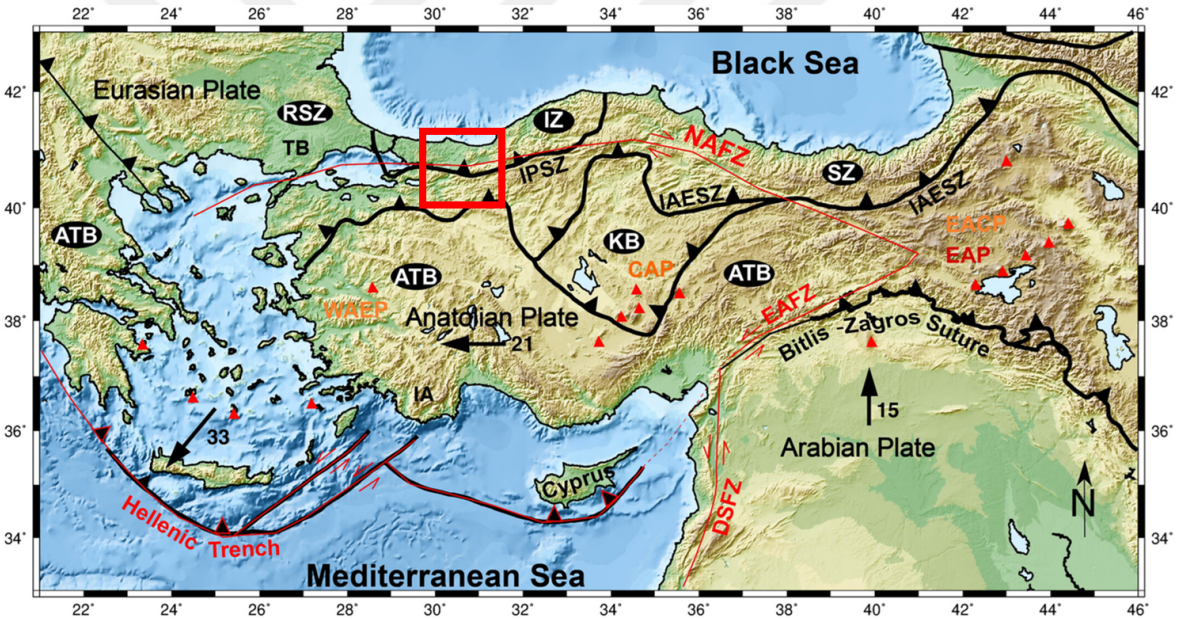

Figure 1.1. Tectonic setting of Türkiye (Wang et al., 2020). Suture zones are shown by the thick black lines (Wang et al., 2020; Okay & Tüysüz, 1999). The late Cenozoic volcanic centers are shown by the red triangles. Major faults and trenches are shown by the red lines.

The NAFZ in Türkiye is an active fault system that spans over 1200 kilometers (Figure 1.1). It is characterized by right-lateral strike-slip motion that enables the westward movement of the Anatolian Plate due to the northward convergence of the Arabian Plate relative to the Eurasian Plate (Şengör & Yılmaz, 1981). In Figure 1.1 late velocities (mm/yr) relative to fixed Eurasia are indicated by the black arrows and

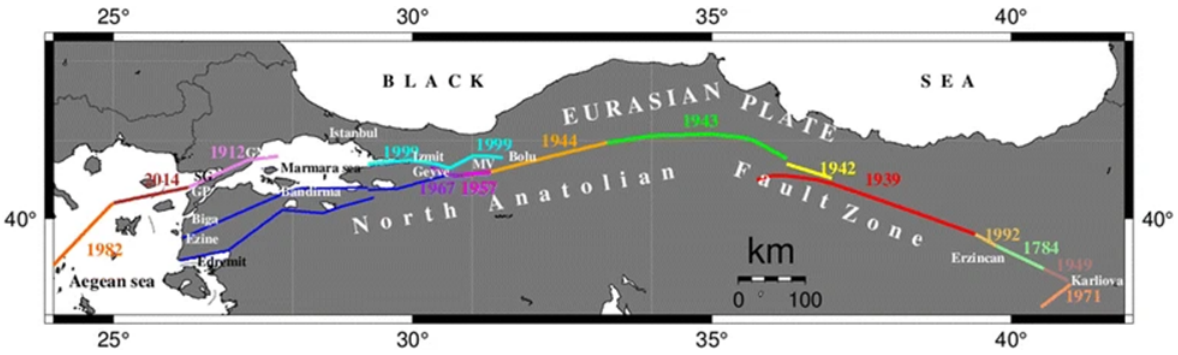

Figure 1.2. Historical earthquakes along NAFZ show the earthquake migration to the west (Pınar et al., 2016). Colored segments represent the major earthquakes and fault ruptures that have occurred along the North Anatolian Fault (NAF) since the December 26, 1939, Erzincan earthquake.

associated numbers (Wang et al., 2020; Reilinger et al., 2006) and the explanation of abbreviations are given in the list above. The NAFZ has been extensively studied regarding its features, seismic activities, fault movements, and deformation patterns (Reilinger et al., 2006; Özener et al., 2010; Eken et al., 2013; Fattahi & Amelung, 2014; Bohnhoff et al., 2016; Havazlı et al., 2021). Historical records indicate it has been responsible for a lot of devastating earthquakes (Figure 1.2), including the earthquakes that occurred in Erzincan (1939), Niksar Erbaa (1942), Tosya (1943), Bolu Gerede (1944), Abant (1957), Mudurnu Valley (1967), as well as the 1999 Izmit and Düzce earthquakes (Ambraseys & Jackson, 2000). These seismic events and the destruction they cause has revealed the importance of conducting studies to understand the fault dynamics, and provide information on fault line behavior in order to mitigate risks.

The behavior of a fault line is subject to change over time. The accumulation of stress on a fault over an extended period and the subsequent release of stress along the fault line during an earthquake are collectively referred to as seismic cycle (Figure 1.3). The sequence is comprised of three phases: interseismic, coseismic, and postseismic deformation. During the interseismic phase, tectonic plates continue to move slowly along the fault, exhibiting a non-localized displacement. The fault remains locked due to loading stress without slipping, resulting in the accumulation of strain energy in the surrounding crust. Geodetic techniques, like GPS and InSAR, are utilized to monitor

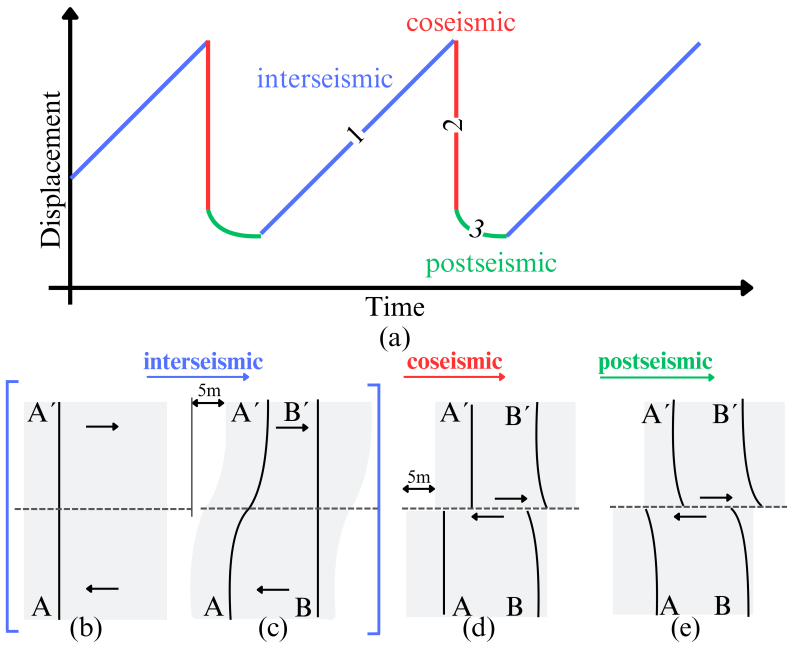

Figure 1.3. Seismic cycle description with using the elastic rebound model of Reid (1910) (modified from Wright, (2002).

deformation and strain buildup during this stage (Savage, 1983). The coseismic phase occurs when the stress built up on a fault exceeds the strength of the fault, releasing energy as an earthquake. This phase is characterized by ground movements along the fault and the generation of seismic waves. The earthquake's intensity is directly linked to the stress released during this phase (Scholz, 2002). After the earthquake, the postseismic phase involves the adjustment and relaxation of the crust. This phase includes aftershocks, gradual slipping along the fault (afterslip), and viscous crust and upper mantle relaxation. The postseismic deformation may persist for months or years after the quake and is monitored through the use of geodetic and seismic data (Marone et al., 1991).

A more comprehensive understanding of the behavior and characteristics of the NAFZ during the interseismic period is crucial for accurately assessing earthquake risks and enhancing preparedness. Therefore, this thesis focuses on the spati-temporal monitoring of surface deformations along the NAFZ in the Düzce region using methods such as InSAR time series analysis and GPS observations and their interpretation by geophysical techniques such as Coulomb stress analysis and seismic tomography.

The purpose of this thesis is to present a thorough analysis of the seismic risks and fault behavior in the Düzce region located along the NAFZ and to better understand why monitoring the surface deformation rate is important. Chapter 1 provides an overview of the NAFZ, emphasizing its geological importance, past seismic activity, and the research goals. Chapter 2 provides an in-depth examination of the study region, specifically focusing on the tectonic context, geological characteristics, and past research undertaken in the Düzce area. Chapter 3 provides a comprehensive analysis of the existing literature, examining important discoveries from recent studies on seismic activity and deformation patterns in the area. This chapter specifically emphasizes the techniques and outcomes of noteworthy research. Chapter 4 discusses the methods used in this research, which includes InSAR time series analysis, Coulomb stress analysis, and data processing techniques. Chapter 5 presents the findings of the investigation, including a thorough examination of the ground deformation and stress variations. The results are supported by the inclusion of figures and tables. Chapter 6 concludes the study by providing a detailed analysis and summary. It compares the findings with past research, evaluates their significance for assessing seismic hazards.

2. STUDY REGION

2.1. Tectonic Setting of Türkiye and the NAFZ

Türkiye's location is at the junction of the African and Arabian plates, making it a highly active area. This collision of plates leads to seismic events that shape the country's topography and structures. The Anatolian Plate moves westward primarily due to pressure from the Arabian Plate pushing northwards and colliding with the Eurasian Plate (Şengör & Yılmaz, 1981). This movement is aided by fault systems like the North Anatolian Fault Zone (NAFZ).

Understanding the geological evolution of areas where tectonic plates have interacted requires an understanding of the link between tectonism and suture zones. Suture zones are boundaries where major tectonic activity has resulted from the merging of former lithospheric plates. The suture, a major metamorphic, magmatic, stratigraphic, and structural boundary in the area, is mostly defined by the fault zone. In Figure 2.1, the tectonic map illustrates the northern Mediterranean region's major continental blocks and sutures. Along with two north-trending transform faults, the NAFZ is a component of a collisional suture that was formerly a plate boundary during the Cretaceous period. (Okay & Tüysüz, 1999).

The NAFZ plays a crucial role in facilitating the westward motion of the Anatolian Plate through complex tectonic interactions. Its high seismic activity levels have made it a target area for studying plate tectonics in this region (McKenzie, 1972; Şengör et al., 1985; Barka, 1996; Stein et al., 1997; Armijo et al., 1999; Bozkurt, 2001). A comprehensive analysis of seismic activity throughout the 20th century, starting with the 1939 Erzincan earthquake and including the 1999 Izmit and Düzce earthquakes, revealed that each event has its own seismic characteristics such as rupture length, slip rates and locking depths (Barka, 1996; Stein et al., 1997). However, the primary mechanism underlying these events was identified as right-lateral strike-slip motion

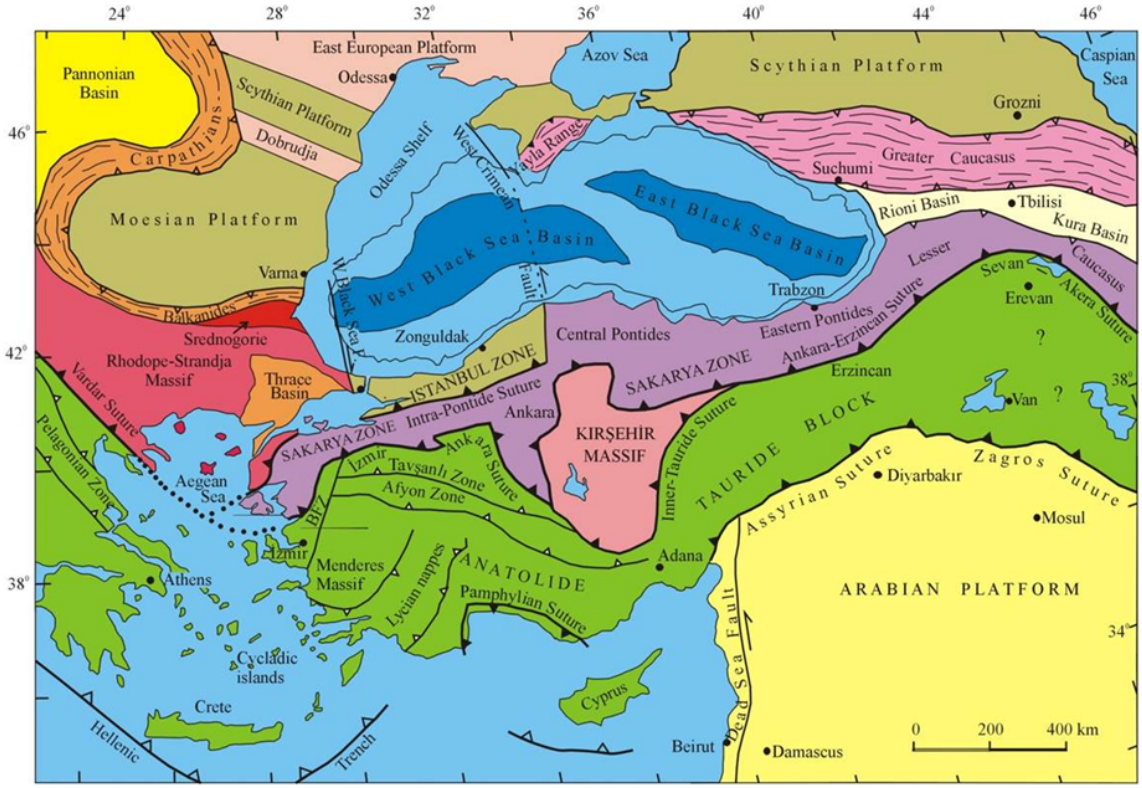

Figure 2.1. Tectonic map illustrating the main continental blocks and sutures in the northern Mediterranean region. Filled triangles reveal the polarity of previous subduction zones. Grey tones highlight the Black Sea's Late Cretaceous oceanic crust. Rewritten in light of Şengör (1984) Okay (1989), and Okay et al. (1994, 1996) (Okay & Tüysüz, 1999)

along this fault system.

Barka (1996) presented a comprehensive perspective on the seismic activity of the NAFZ during the 20th century by outlining the distribution of 1939, 1943, 1944, 1957, 1967, and 1999 earthquakes along the fault. He provided a comprehensive analysis of the rupture lengths, slip rates, and spatial-temporal evolution of these seismic events, emphasizing the interrelationship of big earthquakes throughout the fault line, where each event caused future ones. Barka highlighted the sequential progression of seismic activity, in which the transfer of stress from one segment to another resulted in a succession of significant earthquakes occurring in a very little timeframe (Barka, 1996). Furthermore, Stein et al. (1997) conducted an investigation related to the failures that

have occurred in the NAFZ since 1939. He emphasized the influence of seismic stress on the fault's behavior. The results of their research demonstrated the significance of comprehending stress interactions between fault segments in order to anticipate potential occurrences.

On the other hand, Ambraseys and Jackson (2000) conducted a historical analysis of the NAFZ. The researchers examined earthquakes from the past centuries and explored the factors that affected their distribution along the fault line, which yielded valuable insights into the frequency and magnitude of specific earthquakes. They analized the temporal and spatial patterns of notable seismic events, which unveiled the historical prevalence of heightened activity in certain fault segments compared to others. Their research yielded valuable information regarding the frequency and magnitude of earthquakes in different segments of the NAFZ. Specifically, they found that the eastern Marmara region has experienced more frequent and larger magnitude earthquakes compared to other parts of the fault (Ambraseys & Jackson, 2000). By establishing a correlation between historical data and current seismic readings, they emphasized the significance of comprehending previous seismic activity in order to predict future earthquake patterns along the NAFZ.

Additionally, studies have been conducted to ascertain the timing and process of the NAFZ's formation. In their analysis, Şengör et al. (2005) investigated the evolution of the NAFZ and revealed its significance for the geodynamics of the Anatolian region. Their findings highlight how the NAFZ enabled the westward shift of the plate and the shaping of regional tectonics over millions of years. According to their study, the NAFZ began forming around 13 million years ago during the late Miocene epoch, driven by the collision between the Arabian and Eurasian plates. Furthermore, the study examined the relationship between the NAFZ and other fault systems in the region, providing insight into the complex interactions between various tectonic plates. Şengör et al. (2005) highlighted the significant impact of these interactions on the tectonic evolution of the Eastern Mediterranean and surrounding areas, demonstrating the crritical role of the NAFZ in wider geodynamic processes.

2.2. Geology and Tectonics of the Düzce Region

The Düzce region, situated in the western part of Türkiye, is known for its significant seismic activity, notably highlighted by the strong 1999 Düzce earthquake with magnitude of Mw7.2. This earthquake resulted in extensive damage and loss of life, as documented by Akyüz et al. (2002). In the Düzce region, the Istanbul-Zonguldak, Armutlu-Almacik and Sakarya zones are located from north to south, separated by the Düzce fault and the southern branch of the NAFZ. The Düzce region's geology is characterized by a complex tectonic history influenced by various processes. The area is distinguished by a heterogeneous assemblage of rock types, which reflects its dynamic geological evolution. In particular, the region comprises Paleozoic rocks, Mesozoic ophiolites (a type of oceanic crust), and Cenozoic sedimentary layers. The sedimentary layers found in the Düzce region comprise deposits from both continental and marine environments, indicating periods of subsidence and uplift during the area's geological development. This geological diversity contributes to the intricate tectonic framework of the region. Extensive geological surveys and seismic analyses have identified fault lines within the Düzce basin. Emre et al. (2013) provide insights into the detailed geological structure of the area, emphasizing the presence of fault lines and their role in shaping the region's landscape.

The Düzce region is characterized by the fact thatbifurcation of the NAFZ into two branches from here to the west. This region faces significant seismic risk due to its location on the NAFZ and its complex geological composition shaped by various tectonic processes such as strike-slip faulting, subduction, and continental collision over geological time scales (Şengör et al., 1985; Bozkurt, 2001). The 1999 Düzce earthquake, as documented by Akyüz et al. (2002), ruptured approximately 40 kilometers of the fault, offering valuable insights into fault movements and earthquake hazards. One significant finding from this event was the identification of a right-lateral strike-slip motion with a vertical component, which contributed to understanding the fault dynamics and the associated seismic risk in the region. The ongoing faulting and strain accumulation along the NAFZ continue to increase the seismic risk in Düzce region.

The Düzce earthquake, with a magnitude of Mw6.0, which occurred in 2022, serves as a reminder of the region's seismic activity. Therefore, it is of the utmost importance to conduct continuous monitoring in order to gain a comprehensive understanding of stress distribution for assessing earthquake potential and formulating effective strategies for hazard mitigation.

2.3. Previous Studies in Düzce Region

The Düzce region, situated along the NAFZ, has been undergoing extensive investigation with regard to its geophysical properties, because of the seismic risk that it faces. The objective of the researches is to gain a deeper understanding of the mechanics of faults, the distribution of stress, and the deformation patterns to improve earthquake preparedness and mitigation strategies in this region.

2.3.1. Geodetic Studies

GPS readings have been instrumental in monitoring of changes in the Earth's crust and stress accumulation. In conjunction with Interferometric Synthetic Aperture Radar (InSAR) technology, GPS measurements provide invaluable insights into deformation and strain accumulation analysis. GPS networks are consistently used to monitor ground movements in Düzce region, allowing precise measurements of tectonic motions.

Geodetic measurements are necessary to understand how strain accumulates and is subsequently released along the NAFZ, as highlighted by Reilinger et al. (2000) who utilized GPS data to analyze deformation patterns along the NAFZ in their research and emphasized that the strain increased over time in this area. They assessed ground deformation levels and strain loading by analyzing GPS data collected before and after the 1999 earthquake. The authors identified areas with significant strain accumulation, particularly around the eastern Marmara region and the Düzce segment of the fault, which experienced notable stress increases. Their research revealed a 20% increase in

stress levels in these regions after the 1999 earthquake, identifying critical zones with a higher probability of experiencing future seismic events. Their research highlights the significance of using GPS monitoring to evaluate seismic risks and improve earthquake preparedness (Stein et al., 1997; Bozkurt, 2001; Reilinger et al., 2000). Understanding these connections between stress and strain is crucial for fpredicting possible earthquakes and for implementing efficient measures to reduce their impact.

Recent studies have focused on utilizing both GPS and high-resolution InSAR data to examine deformation processes in greater detail (Wright et al., 2004; Aslan et al., 2019). In their 2019 study, Aslan et al. employed the use of GPS technology in conjunction with high-resolution InSAR data in order to investigate surface movements along the NAFZ (Figure 2.2). In Figure 2.2, on the top, the mean velocity fields for the period 2014–2017 were derived using the PS-InSAR time series analysis of Sentinel 1A/B descending track 138. These velocity fields represent the line-of-sight velocities and are expressed in a reference frame fixed to Eurasia. The mean line-of-sight velocity fields for the period 2014-2017, acquired from PS-InSAR time series analysis, are presented for Sentinel 1A/B ascending tracks 58 (a) and 160 (b), as well as for TerraSAR-X ascending track 24 (c) for the period 2011-2015. These velocity fields are depicted in a reference frame set to Eurasia. Their objective was to analyze long-term ground deformation patterns captured by GPS and InSAR measurements. The study discovered specific areas along the NAFZ where movement was observed, with deformation rates reaching up to 20 mm/year in certain sections. This provided detailed information about the ongoing deformation processes. Aslan et al. (2019) specifically examined the Izmit segment of the NAFZ, emphasizing noteworthy displacements in this region. The researchers analyzed the consequences of these discoveries on possible upcoming seismic events in the Izmit area, highlighting the need of understanding fault behavior in order to evaluate regional earthquake hazards. To understand these patterns of deformation is essential for forecasting upcoming seismic occurrences and developing efficient ways to reduce their impact.

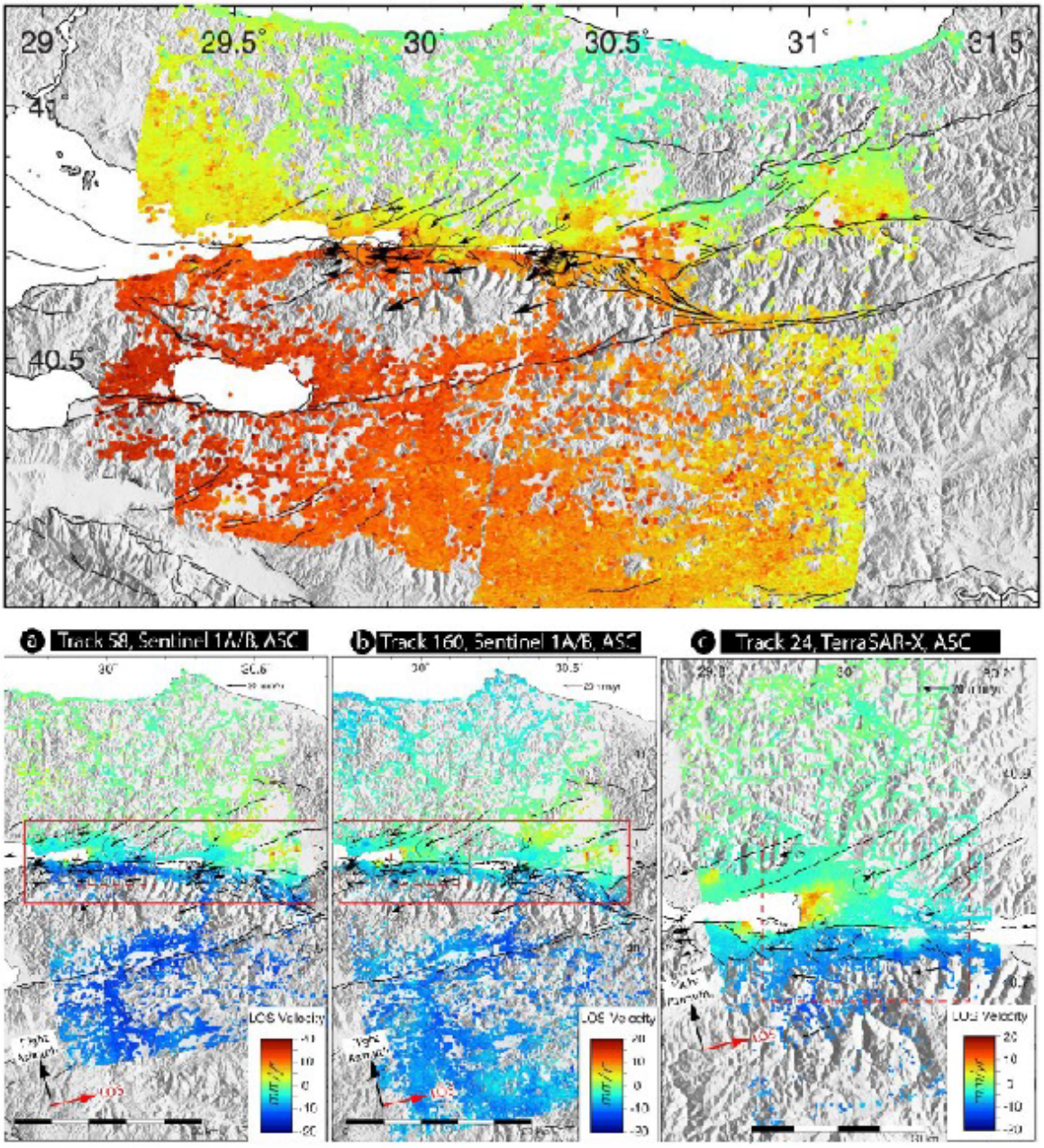

Figure 2.2. PS InSAR models on the İzmit and Düzce Region.

Weiss et al. (2020) conducted an extensive investigation on surface velocities and strain rates across the Anatolian region. They utilized data from Sentinel-1 InSAR and GNSS to specifically examine the North Anatolian Fault (NAF). According to the research, which analyzed data from 2014 to 2019, the Anatolian plate has been moving towards the west with a notable velocity of around 20-25 mm per year in relation to the Eurasian plate (Figure 2.3). The motion was characterized by a distinct change in velocity across the NAF and significant build-up of strain along both the North Ana-

tolian Fault (NAF) and the East Anatolian Fault (EAF). The integration of InSAR and GNSS data yielded improved resolution and precision in mapping these tectonic displacements. The study's Figure 2.3 illustrates the tectonic configuration of Anatolia, showcasing GNSS velocity vectors and line-of-sight velocities from Sentinel-1. In Figure 2.3b ascending and Figure 2.3c descending track Sentinel-1 line-of-sight (LOS) velocities are provided, together with LiCSAR frame boundaries. Blue color represent negative relative motion towards the satellite, whereas red color represent positive relative motion away from the satellite. The color scale is identical in Figure 2.3b and Figure 2.3c. The figure clearly demonstrates the counterclockwise rotation of Anatolia and notable movements along the NAF and EAF. This effectively demonstrates the success of the methods used in accurately capturing these complex dynamics. This study highlights the crucial importance of high-resolution geodetic data in comprehending tectonic processes and evaluating seismic risks in the area.

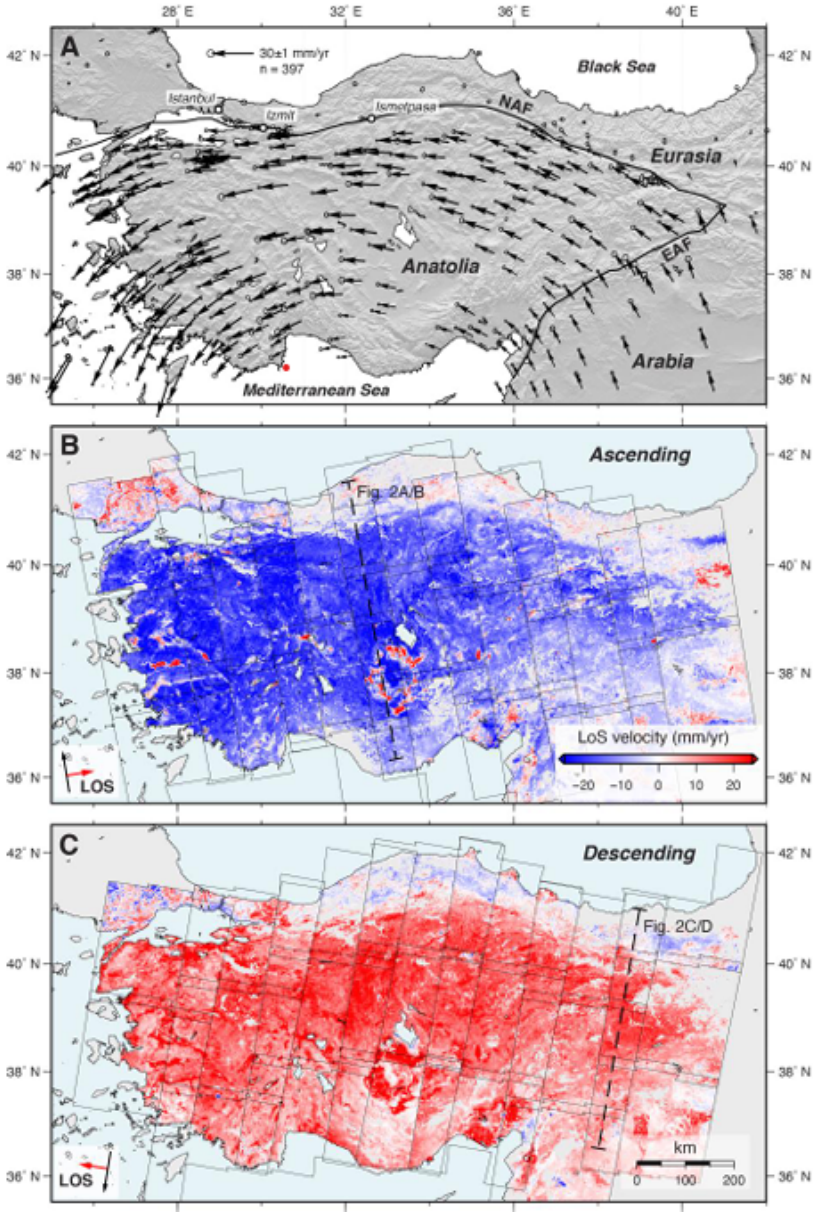

Figure 2.3. The tectonic setting of Anatolia and the interseismic surface velocities (Weiss et al., 2020), measured in a reference frame that is fixed to Eurasia. The GNSS velocity vectors from England et al. [2016] and Nocquet [2012] demonstrate the counterclockwise rotation of Anatolia and Arabia in relation to Eurasia.

2.3.2. Geophysical Studies

Seismic tomography is a technique that creates images of the Earth's subsurface structure by analyzing the travel times of waves generated by earthquakes or artificial

sources. This method provides information about layers that capture variations in seismic velocity due to differences in temperature, composition and other physical properties of rocks.

Wang et al. conducted a study in 2020 where they used three-dimensional seismic tomography to examine seismic anisotropy and velocity (Vp) in the crust and uppermost mantle beneath Turkey, specifically in the Düzce area. The objective of this study was to enhance our comprehension of the correlation between seismic velocity anomalies and fault structures, while also identifying variations in rock composition and fluid content. Wang et al. (2020) identified notable anisotropic properties and fluctuations in seismic velocities, suggesting complex tectonic interactions and the existence of rock zones saturated with fluids and fractured. The study found that the Düzce region has lower seismic velocities than the surrounding areas, indicating the presence of possible weak zones and areas where strain accumulates. The significance of seismic tomography in detecting crucial areas that may impact the initiation and spread of earthquakes in the region is emphasized by these findings. Their findings yielded crucial information regarding the subterranean structure of the Düzce region and increased our comprehension of the geodynamic factors influencing seismic activities in this area.

Barka (1999) provided a comprehensive analysis of seismic activity and fault dynamics in the Düzce region, with special emphasis on the 1999 Düzce earthquake. The study provided deep insights into the characteristics of earthquake rupture and the distribution of Düzce earthquake aftershocks. He highlighted the critical importance of understanding fault segmentation and the role of different fault segments in the earthquake rupture process. The study emphasized the need for continuous monitoring and ongoing research to better understand seismic risks. The analysis utilized a range of geophysical techniques, such as seismic reflection and refraction surveys, along with aftershock monitoring utilizing a network of seismometers. These techniques revealed detailed images of the subsurface structures and the dynamics of the fault during and following the earthquake. The seismic reflection data was crucial in determining the

exact position and size of the fault rupture, while the maps showing the distribution of aftershocks offered valuable information on how stress was redistributed along the fault. One important discovery was the recognition of a complex rupture pattern that affected many fault segments, leading to a major impact on aftershock activity and stress transfer processes. The significance of geophysical measurements in understanding the dynamics of seismic events and assessing the associated risks are emphasized by these results. In their 2005 study, Barış et al. employed three-dimensional seismic tomography to examine seismic velocity (Vp) and the ratio of P-wave velocity to S-wave velocity (Vp/Vs) in the upper crust of the Marmara region. The objective of this research was to gain insight into the correlation between seismic velocity anomalies and fault structures identifying variations in rock composition and fluid content. These factors are of great importance for comprehending fault mechanics and processes related to earthquake generation. The researchers developed a comprehensive three-dimensional model of the subsurface, utilizing data from a network of seismometers. The study of Barış et al. in 2005 emphasizes the intricate relationship between geological structures and tectonic activities in the Marmara region. In the Düzce region, lower seismic velocities and greater Vp/Vs ratios were observed, which suggest the presence of fluid-saturated and fractured rock zones. These anomalies indicate the presence of potential roughness or areas where there is a large build-up of strain. These are critical for understanding nucleation process in this region.

Another geophysical technique employed in the Düzce area was magnetotelluric (MT) studies. The MT technique, which is a natural sourced electromagnetic method, is instrumental in mapping the subsurface electrical conductivity, thereby providing insights into the structure of the Earth's crust. By collecting MT data along two profiles crossing the branches of the NAFZ in the Düzce region, Kaya et al. (2009) aimed to explore the correlation between variations in conductivity and geological features, fluid presence, and to investigate potential implications for earthquake hazards. Significant variations in conductivity levels were identified from west to east profile. These variations suggest the potential presence of fluids and weak zones between the northern and southern branches of the NAFZ in the Düzce region. These fluids could

potentially impact fault behavior and seismic activity. Moreover, the elevated resistivities observed at the eastern profile are consistent with the higher seismic velocities observed in the eastern part of the 1999 earthquake epicenter (see Figure 2.4). The resistivity models for (a) DW and (b) DE profiles were derived by jointly inverting the TE and TM mode data. The transition of colors in models, ranging from red to blue, indicates a increase in resistivity. The circles depict areas of aftershocks, with sparse dots representing regions of few aftershocks and dense dots representing regions of many aftershocks. These areas are located beneath the western and eastern sides of the epicenter, respectively. This research plays an important role in understanding the fault mechanics and assessing hazards in the Düzce region, as conductivity models provide valuable information on how the fault zone behaves in relation to existing features and earthquake occurrences, and identify areas where stress can accumulate.

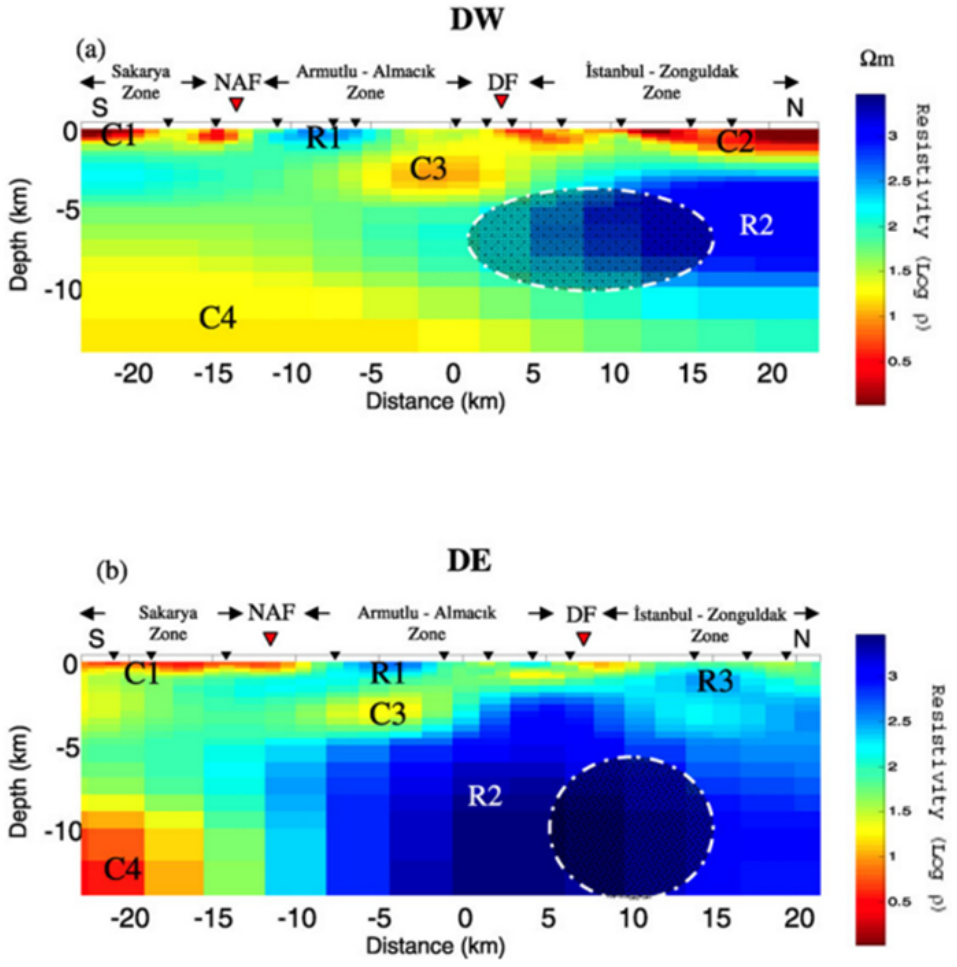

Figure 2.4. Models of magnetotelluric profiles on the Düzce Region (Kaya et al., 2009). The black triangles indicates MT stations. The red triangles represent the NAF and the Düzce fault, in that order, from a southern to northern direction. The circles depict areas of aftershocks, with sparse dots representing regions of few aftershocks and dense dots representing regions of many aftershocks.

3. METHODOLOGY

This study is mainly based on Interferometric Synthetic Aperture Radar (InSAR) time series analysis, which allows monitoring of surface deformations over large areas at specific time intervals. InSAR is a radar imaging geodetic technique that uses satellite radar imagery to precisely detect ground movement over areas ranging from tens to hundreds of kilometers (Bamler et al., 1998; Rosen et al., 2000). Therefore, we utilized the InSAR method for spatio-temporal deformation analysis of the North Anatolian Fault Zone (NAFZ) in the Düzce region.

This section provides an overview of the principles of Synthetic Aperture Radar (SAR) and InSAR methods, outlining the data processing workflow. It also provides an explanation of the time series analysis (SBAS) technique that was used in this thesis. Additionally, it describes the geophysical methods utilized to understand the dynamics of the NAFZ in order to better interpret the deformation in the Düzce region.

3.1. Geodetic Methods

3.1.1. Interferometric Synthetic Aperture Radar (InSAR)

Although SAR systems such as airborne (e.g., UAVSAR [Hensley et al., 2009; Rosen et al., 2006; Madsen et al., 1995] and ground-based SAR [Tarchi et al., 2003; Monserrat et al., 2014; Crosetto et al., 2016] are widely used to study ground deformation analysis, satellite-based SAR images are currently the most widely employed. Figure 3.1 shows the satellite-based SAR data acquisition geometry, illustrating how SAR-equipped satellites collect radar data The geometry includes key parameters such as azimuth (the flight direction of the satellite), range (the line-of-sight distance between the satellite and the ground), pixel resolution (the size of the ground area represented by each pixel in the SAR image), nadir (the point directly beneath the satellite), and overall resolution, which determines the level of detail in the acquired images. These

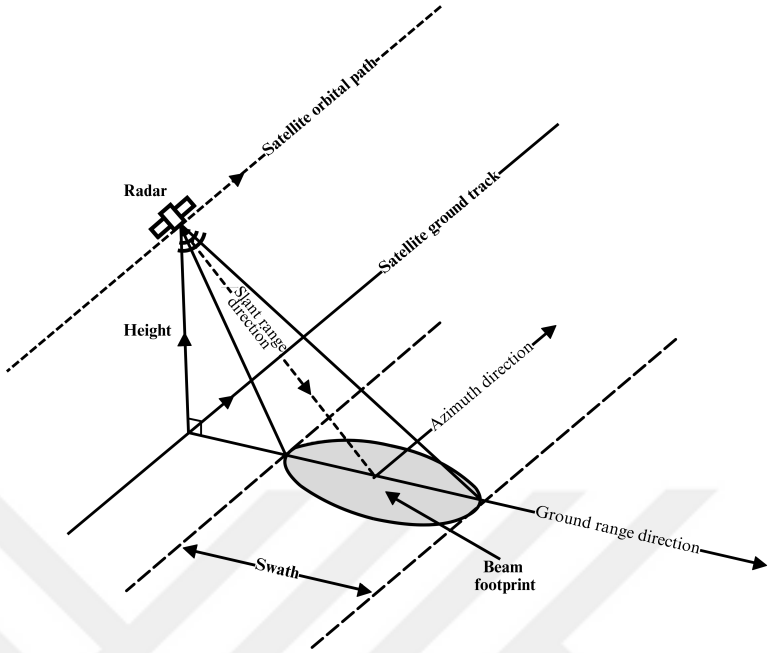

Figure 3.1. Synthetic-aperture radar acquisition representation modified from Anderlini, (2014).

parameters are critical for understanding the spatial accuracy and quality of the SAR data.

SAR sensors use different frequency bands to transmit and receive radar signals, each with different penetration capabilities into vegetation and soil. These bands are categorized based on their wavelengths λ, which can range from low frequency L-band (is $\sim 15-30$ cm, f is $1-2$ GHz) to C-band (is $\sim 3.75-7.5$ cm, f is $7-8$ GHz), and the high frequency X-band (is $\sim 2.5-3.1$ cm, f is $8-12.5$ GHz). Lower frequency bands (e.g., L-band) penetrate deeper into vegetation, making them suitable for applications like monitoring soil moisture or detecting subsurface features, while higher frequency bands (e.g., X-band) provide higher resolution images, distinguishing smaller objects on the ground compared to lower frequency bands and enabling detailed surface mapping and change detection. In this thesis, C-band Sentinel-1 data were selected in order to examine spatio-temporal deformation on the NAFZ in Düzce region.

Between 2014 and 2016, the European Space Agency launched the Sentinel-1 satellite constellation, consisting of the Sentinel-1A and Sentinel-1B satellites equipped

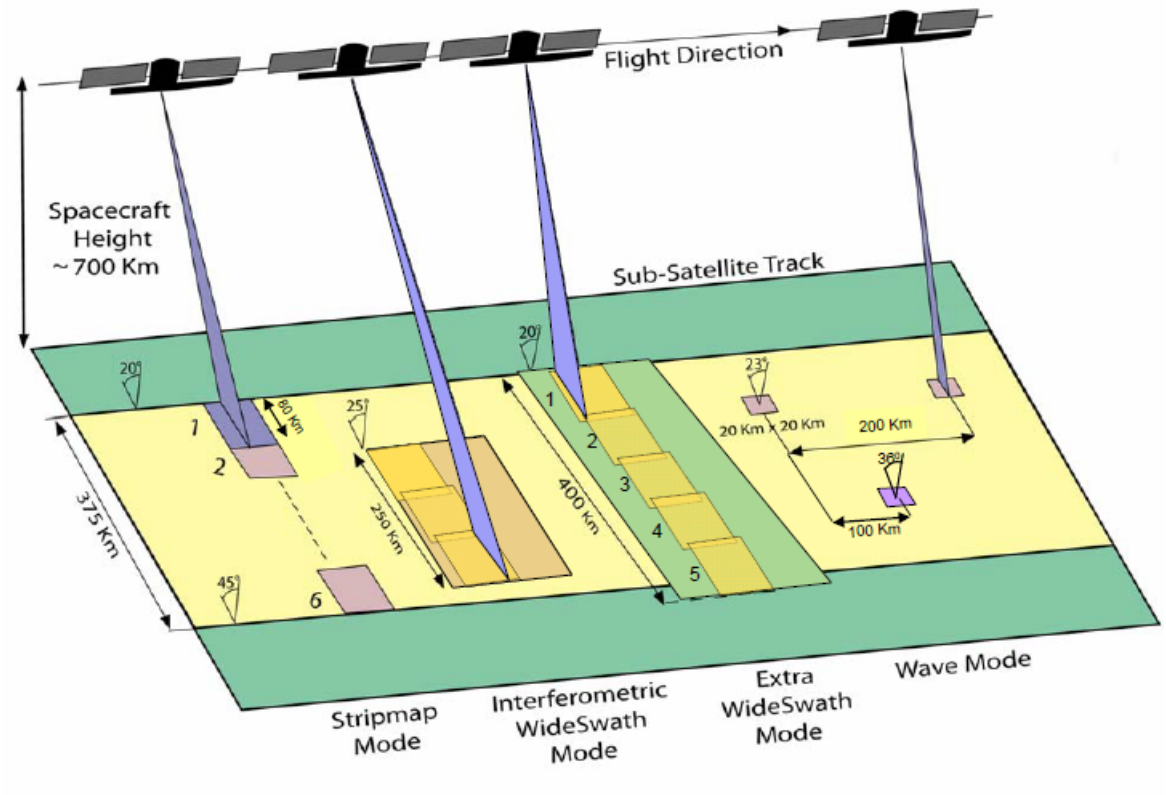

Figure 3.2. SAR acquisition modes representation (taken from ESA's website). Stripmap mode, Interferometric WideSwath mode, Extra WideSwath mode and Wave mode are described from left to right.

with C-band SAR technology. These satellites orbit the Earth in a polar sun-synchronous orbit, providing global coverage with precise transit times. Since SAR instruments operate in several modes, including stripmap, spotlight, and scanSAR, each offering different trade-offs between swath width, resolution, and coverage, SAR images can be acquired in one of these modes (Figure 3.2). Operating in the Terrain Observation Synthetic Aperture Radar with Progressive Scans (TOPS SAR) mode, Sentinel-1 satellites enable wide-area imaging while maintaining resolution levels useful for InSAR applications due to their accuracy over large regions. Figure 3.3 illustrates the TOPS acquisition geometry, which is used in this thesis, and shows how this mode takes advantage of sensor motion to utilize overlaps between bursts and sub-swaths, improving acquisition efficiency and coverage consistency (Figure3.3).

In the process of InSAR data an interferogram is created by analyzing phase

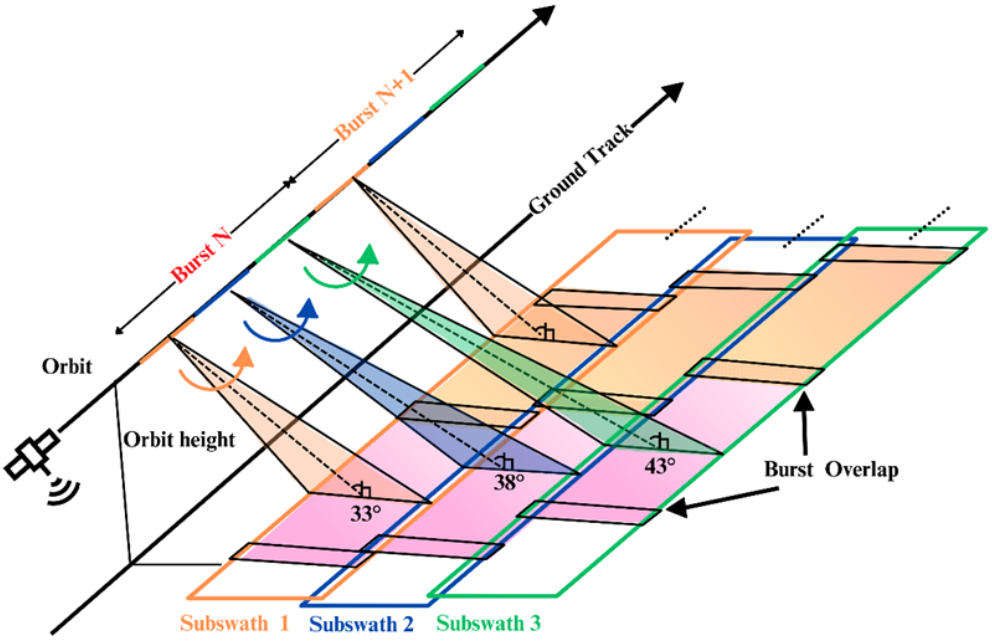

Figure 3.3. Sentinel-1 TOPS Acquisiton Geometry modified from Yu et al. (2019).

differences in radar signals from two SAR images taken at specific times at the location to detect ground movements. This technology is particularly useful for monitoring changes on the Earth's surface along active fault lines, such as the NAFZ, and in volcanic areas like Mount Etna, or in regions experiencing subsidence or uplift as in India or Iran (Gabriel et al., 1989; Massonnet & Feigl, 1998). In the 1990s, InSAR emerged as a tool to study tectonics. Initially used to measure groundwater-induced deformation in California (Gabriel et al., 1989), InSAR has since been widely applied to examine phenomena such as volcanoes (Hooper et al., 2004; Lu et al., 2007; Poland et al., 2006), landslides (Colesanti & Wasowski, 2006; Farina et al., 2006; Rott et al., 2009), earthquakes (Fialko et al., 2005; Bürgmann et al., 2000; Jónsson et al., 2002) and aseismic deformation (Hoffmann et al., 2003; Cakir et al., 2005; Wang et al., 2012).

In general, the fundamental concept of InSAR is based on evaluating the phase information of radar signals, which is influenced by various factors including topography, atmospheric conditions, and ground movements between radar image acquisitions. To obtain deformation data accurately, it is necessary to extract the topography from the interferogram, for which a digital elevation model (DEM) is used. The resulting phase change reflects the surface displacement in radian unit, which is then converted

into the absolute unit of the ground movement. The link between phase change and displacement is expressed as:

$$\Delta\phi = (4\pi/\lambda)\Delta d, \tag{3.1}$$

where $\Delta\phi$ represents phase change, λ stands for the radar wavelength, and Δd denotes the ground movement (Hanssen, 2001; Rosen et al., 2000). This formula forms the basis for precise deformation analysis in InSAR, enabling measurements at millimeter-level accuracy.

Advanced InSAR techniques like Small Baseline Subset (SBAS) and Persistent Scatterer Interferometry (PSI) further enhance deformation investigation capabilities. SBAS utilizes a sequence of interferograms with spatial baselines to improve deformation measurement quality by reducing decorrelation effects (Berardino et al., 2002). On the other hand, PSI focuses on stable scatterers that maintain coherence over time, providing reliable time series data for deformation analysis (Ferretti et al., 2001). These methodologies are facilitated by different software tools to generate deformation maps and compute deformation rates crucial for understanding tectonic processes and assessing seismic risks (Yunjun et al., 2019; Fattahi & Amelung, 2013). The software packages used to perform InSAR data analysis such as GMTSAR, DORIS, GAMMA, SARSCape, StaMPS, SNAP, and GIAnT vary in complexity and specific functionalities. In this thesis, InSAR Scientific Computing Environment-2 (ISCE2) software and the Miami INsar Time-series software in PYthon (MintPy) packages were used to generate deformation time series and determine deformation rates during the analysis of InSAR data.

3.1.2. Processing Steps for InSAR

The analysis of InSAR data requires several significant processes to accurately measure ground displacement. The main processing steps include data collection, image alignment (coregistration), interferogram generation, phase unwrapping, and time

series analysis.

SAR data, such as Single Look Complex (SLC) images, has complex values that include both amplitude (magnitude) and phase information. Although the primary purpose of phase information in InSAR operations is to measure ground displacement, the magnitude/intensity images can also offer useful insights into the structural properties of the region. For instance, the magnitude image can effectively emphasize characteristics such as urban areas, vegetation, and water bodies, while the phase image is critical for identifying subtle ground motions. Figure 3.4 is an example SAR image of Mount Vesuvius in Italy.

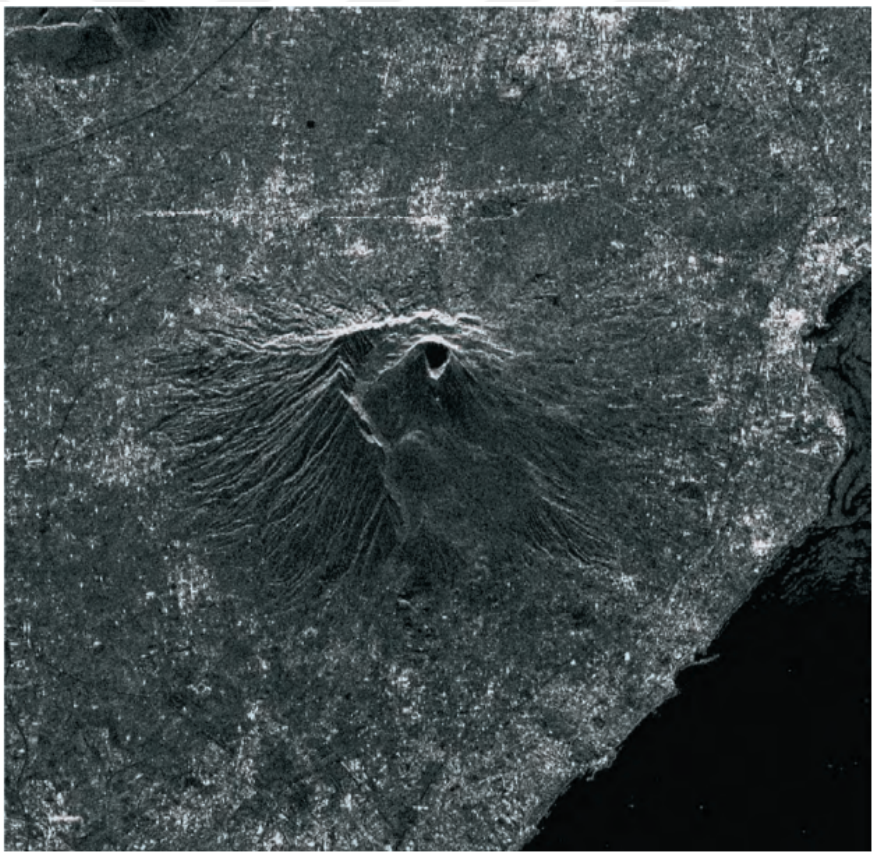

Figure 3.4. An ERS-2 Synthetic Aperture Radar (SAR) image of Mount Vesuvius in Italy, captured and identified by ESA. The image exhibits a vertical slant range direction, with the near range being in the upper section of the image. Higher degrees of brightness are indicative of more intense backscattered radiation.

Coregistration is crucial for aligning the first and the second radar images properly to ensuring ground position represented accurately in each image and for generating high-quality interferograms. The Enhanced Spectral Diversity (ESD) co-registration method is commonly used to improve the accuracy of aligning images for Sentinel-1 TOPS data (Fattahi et al., 2017). ESD is a method that uses the inherent spectrum diversity in SAR data to improve the alignment of images. This approach involves examining the phase information across several sub-swaths in order to achieve precise alignment.

The primary stages of ESD encompass spectral analysis, alignment, refinement. Spectral analysis is conducted on the bursts of Sentinel-1 data in order to derive phase information. Alignment is utilizing the collected phase information to achieve more precise alignment of the images compared to conventional approaches. In the refinement stage, the alignment is improved by iteratively reducing the phase discrepancies between bursts.

Coregistration typically involves the initial coarse alignment, fine alignment, precise alignment and verification. Coarse alignment is achieved by utilizing orbital data and geometric modifications to establish a preliminary alignment of the images. Precise alignment stage is the stage that employs cross-correlation algorithms to correctly match characteristics between the images. In verification stage, the alignment is confirmed by assessing the coherence of phase information across the photos. After accurately aligning the images, an interferogram is created by computing the phase discrepancy between the two images. This interferogram displays the patterns of ground displacement and is critical for InSAR analysis.

Once the images are aligned, an interferogram (Figure 3.5 and Figure 3.6) is generated by calculating the difference in phase between the aligned radar images. This process is performed by multiplying the complex value of each pixel of the first image by the conjugate complex of the corresponding pixel of the second image. This interferogram provides information on the ground movement between the times the

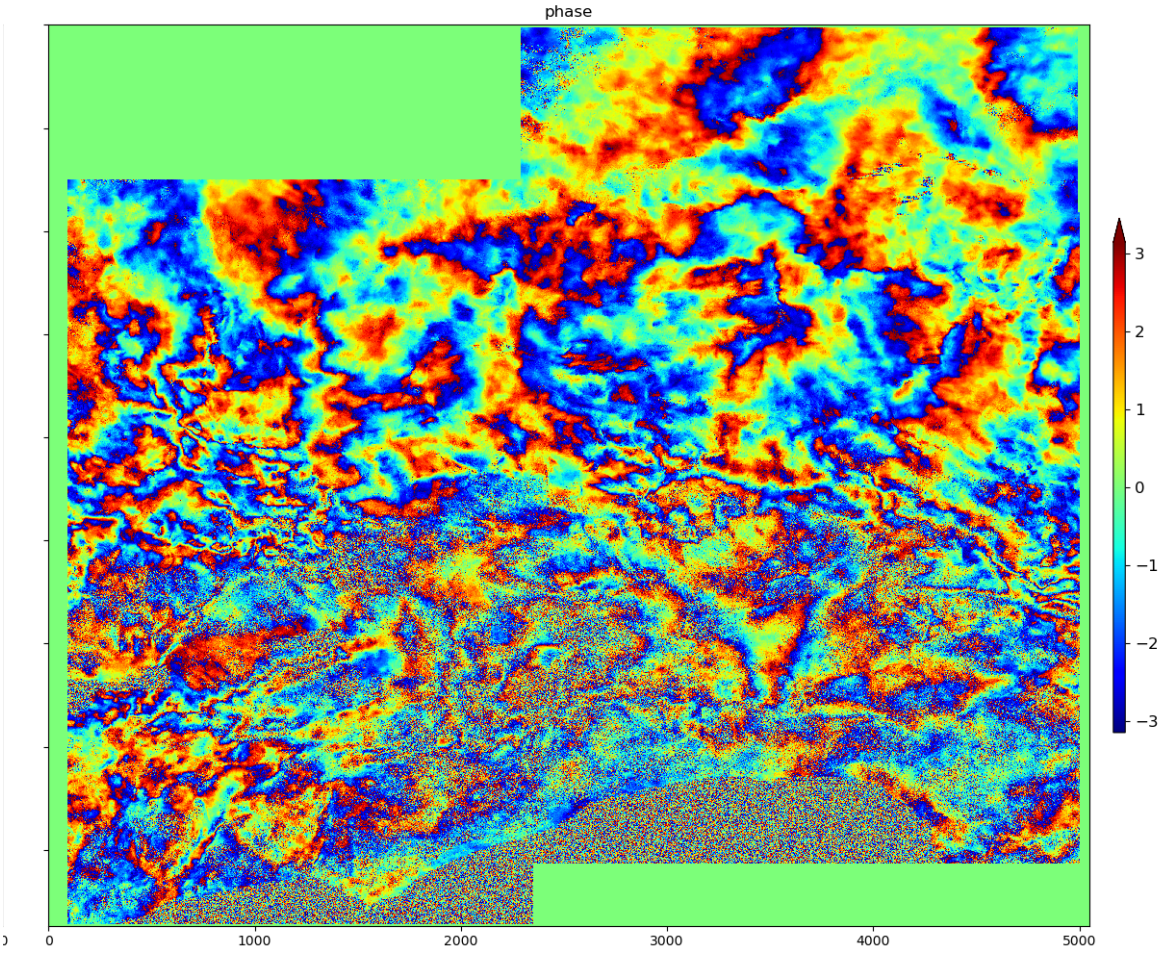

Figure 3.5. Interferogram example obtained from ascending orbit data.

images were taken. The phase difference, as shown in Equation 3.1 is measured in radians and changes based on variations in the distance between the satellite and Earth. The resulting interferogram not only highlights displacement but also reveals subsidence, uplift, or horizontal shifts in the ground. In addition, it is important to apply a filtering process to the interferogram in order to reduce noise and improve the clarity of the signal. This is commonly achieved by using techniques like Goldstein filtering (Goldstein & Werner, 1998).

The next step is phase unwrapping process. The phase data obtained from interferogram is initially constrained between $-\pi$ and $+\pi$ radians, leading to discontinuities that need to be resolved to determine the absolute displacement values. Phase unwrap-

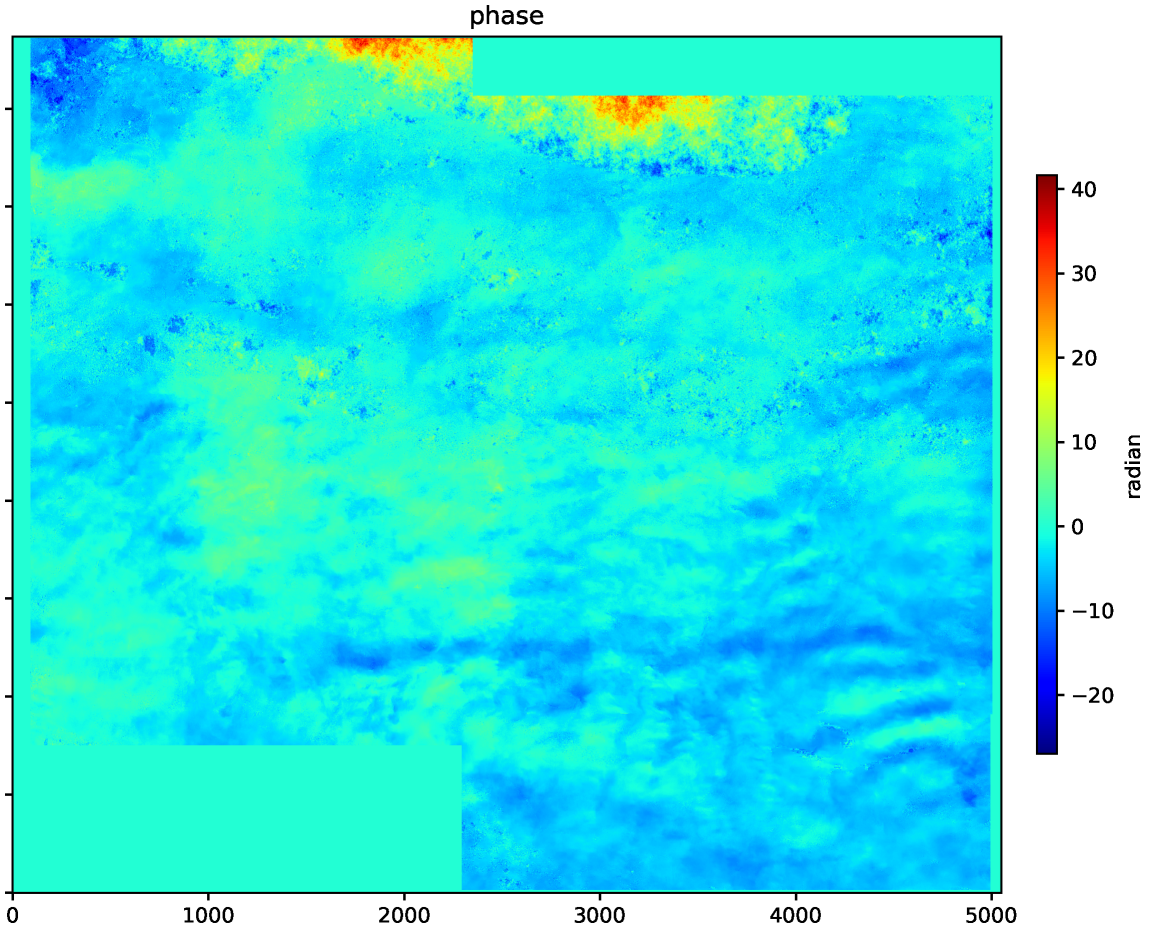

Figure 3.6. Example of an ascending orbit unwrapped interferogram.

ping is crucial to smooth these irregularities and create a continuous phase map. Several techniques, such as the Minimum Cost Flow (MCF) and Statistical cost Network flow Algorithm for Phase Unwrapping (SNAPHU) methods, are utilized for this purpose (Chen & Zebker 2002).

3.1.3. Time Series Analysis

Time series analysis is conducted using a stack of interferograms to track the changes in ground deformation over a specified time interval. The Small Baseline Subset (SBAS) method is commonly employed for this task. Figure 3.7 describes the generation of interferogram stack and SBAS-InSAR workflow. SBAS selects an optimized set of radar image pairs (interferograms) with small spatial and temporal baselines to

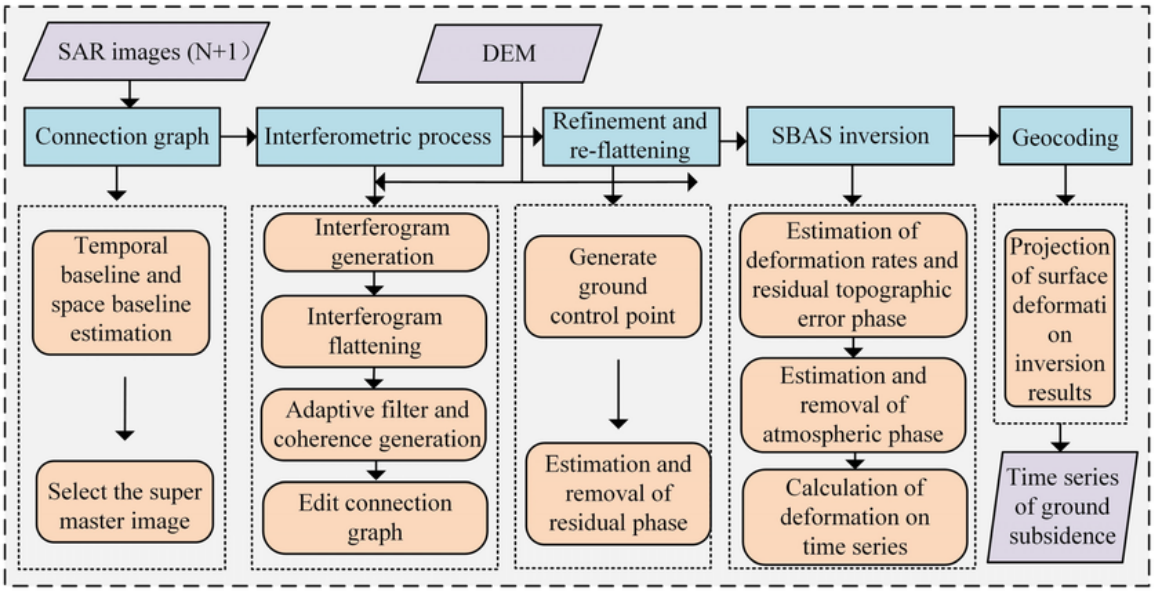

Figure 3.7. Interferogram stack generation and SBAS-InSAR basic processing workflow obtained from Liu et al. (2023).

form an efficient interferogram network. This careful selection providing high temporal coherence between the interferograms reduces decorrelation effects such as atmospheric decorrelation and improves signal quality and reliability of the deformation calculation (Berardino et al., 2002; Lanari et al., 2004). In the time series analysis, the network of interferograms is subject to Singular Value Decomposition (SVD) to separate the data (phase differences) into coherent and incoherent, real deformation and noise, components that capture the deformation signals. The application of SVD helps to filter out noise, enhancing the accuracy of deformation measurements, as discussed in studies Cavalie et al. (2007) and Fattahi et al. (2017). This analysis offers insights into deformation rates and their temporal variations, essential for comprehending the underlying phenomena like seasonal variation or slow deformation.

Subsequently, a network inversion method, a least squares inversion, is conducted on the decomposed data to reconstruct the time series of deformation. This step involves estimating deformation parameters such as displacement rates and temporal changes for each pixel in the radar images for all selected interferograms. Temporal and spatial filtering techniques are employed to refine the time series further and remove

noise. These filters play a role in isolating ground deformations from potential sources of interference, such as atmospheric disturbances (Havazli et al., 2020; Yunjun et al., 2019).

The forward model used to find the deformation parameters in inversion process is shown below:

$$\mathbf{d} = \mathbf{G}\mathbf{m} + \mathbf{n}, \tag{3.2}$$

where $\mathbf{d}$ is the vector of observed phase differences, $\mathbf{G}$ is the design matrix containing the temporal and spatial baselines, $\mathbf{m}$ is the vector of deformation parameters to be estimated, and $\mathbf{n}$ is the noise vector.

3.2. Geophysical Methods

Geophysical methods serve as tools that use physical parameters of the Earth to study structural properties of the fault zones and seismic hazards associated with fault activity, which are prevalent in geologically dynamic regions. In this thesis, methods such as Coulomb stress analysis, seismic tomography and earthquake relocation analysis were utilized to better evaluate deformation rates obtained from InSAR data.

3.2.1. Coulomb Stress Analysis

The study of Coulomb stress is essential for understanding how stress patterns in the Earth's crust change as a result of fault movements and various tectonic activities. This method is based on the determination of the Coulomb failure stress, which also takes into account the normal and shear stresses on a fault surface. By analyzing changes in Coulomb stress levels, scientists can identify areas that may experience higher or lower earthquake probabilities and help assess and manage hazards. Coulomb stress analysis reveals how an earthquake-induced stress change can trigger or inhibit events on nearby faults. The calculated Coulomb stress is represented as $\Delta\sigma_f$, given

below:

$$\Delta\sigma_f = \Delta\tau + \mu(\Delta\sigma_n + \Delta P), \tag{3.3}$$

where $\Delta\tau$ is the change in shear stress, μ is the coefficient of friction, $\Delta\sigma_n$ is the change in normal stress, and ΔP is the pore pressure change.

Researches on Coulomb stress change has significantly improved our understanding of seismic activity. King et al. (1994) laid the groundwork for calculating Coulomb stress by showing how stress changes resulting from fault movement can affect the seismic cycle. Their study highlighted the significance of stress interactions in the temporal propagation of earthquakes. Further research performed by Parsons et al. (1999) used Coulomb stress modeling on the San Andreas Fault system to reveal how past earthquakes redistribute stress along the nearby faults and affect the seismic activity. This method has played an important role in predicting earthquake risks and understanding fault interactions. Stein (1999) further explored the concept of stress triggering by examining how static stress changes impact aftershock patterns. His research revealed that areas, where Coulomb stress is concentrated, are linked to the locations where aftershocks occur, providing a tool for understanding post-earthquake events.

In addition to understanding the stress distribution following a tectonic event on fault lines, Coulomb stress analysis has applications in other geophysical studies. Fialko et al. (2005) used this technique to study stress changes associated with eruptions linked to fault movements and seismic events in volcanic areas. Their discoveries emphasized the interconnected nature of volcanic activity to nearby earthquakes.

Overall, Coulomb stress analysis is a powerful tool for investigating how earthquakes are triggered and how stresses interact within the crust, potentially triggering or inhibiting further seismic activity. By combining this approach with InSAR and GPS data, scientists can acquire insights into mechanics of faulting and deformation, aiding to improve seismic risk assessments.

4. DATA & DATA PROCESS

In this research, the Small Baseline Subset (SBAS) InSAR time series method is used to calculate surface deformation. This section includes the type of data and data acquisition used in InSAR time series analysis, the method of time series data analysis, and the software and tools used.

4.1. Data Acquisition

C-band Sentinel-1 Single Look Complex (SLC) data, which had already undergone some corrections, like Doppler correction, were downloaded from the NASA Alaska Satellite Facility to gather data for the study. The descending orbit data covers track 65 and frames 454, 455, 459, and 460, while the ascending orbit data covers track 160 and frames 125, 127, 130, and 132. Due to limitations in processing T65 F455 frame data alone, two adjacent frames are stitched together to accurately capture deformation patterns.

For the analysis of the descending data, we combined adjacent frames 454-459 and 455-460, similarly, for ascending data, frame number 125-130 and 127-132 are stitched to widen the area of interest to latitude 40°N and 41°N and longitude 30.5°E and 31.6°E. Interseismic deformation calculations were based on data from 2014 up to the Mw6.0 Sarıdere Gölyaka Düzce earthquake on November 23, 2022, using 755 descending and 644 ascending orbit images.

To flatten the data and project it onto two planes, we utilized Digital Elevation Model (DEM) information sourced from the Shuttle Radar Topographic Mission (SRTM) at a resolution of 3 arc seconds (90m). The DEM chosen for ISCE2 processing extended by one degree beyond the region of interest at latitude 40°N and 41°N longitude 30.5°E and 31.6°E to facilitate edge interpolation and minimize errors.

Apart from the DEM, incorporating orbit corrections was crucial in data processing. Hence, we downloaded orbit files corresponding to ascending and descending orbits within the time frame.

Calibration data for dates that needed calibration were also downloaded from the ESAs Copernicus website.

4.2. Interferogram Generation & Stack

In order to visualize how the region of interest deformed annually, it was necessary to convert the data into a stack covering a time period. This task was accomplished using the ISCE2 software and its associated tools. In addition to utilizing the software, it was essential to determine the processing parameters with precision and efficiency. Three connections between the data were initially established, with the 'geometry' method employed for coregistration purposes.

After going through this process, it became clear that the level of coherence was significantly lower and therefore there was significant information loss as a result of masking in the velocity model when interferograms were processed in MintPy. To address this issue, the connections between interferograms were increased to five. The data underwent processing again using the 'geometry' approach. Opting for coregistration with the 'geometry' method in stackSentinel within ISCE2 software involves a series of eleven steps;

1. The tool unpacks the topographic reference data, which provides terrain details as a baseline for comparing images and preparing them for processing. 2. Next, Single-Look Complex (SLC) images are unpacked. These SLC images contain amplitude and phase information for generating interferograms and aligning them with the reference image. 3. The tool then determines the baseline, which signifies the distance between satellite positions during image acquisition to grasp the image geometry and ensure data consistency. 4. Geographic coordinates are converted to radar coordinates for

each burst by performing geo2rdr step to achieve alignment within the radar coordinate system, which is crucial for image matching. 5. Resampling is carried out to adjust burst resolution and alignment, ensuring all bursts are on a grid for combination. 6. The tool selects parts of the image stack based on coherence thresholds, temporal baseline, and spatial baseline, discarding any irrelevant sections to ensure clean data for processing. This selection helps in maintaining high-quality data by filtering out images with poor coherence or large baselines that might introduce errors. 7. The reference and secondary SLC images are combined to create interferograms, which are crucial for comparing data and detecting changes over time. 8. For each burst, an interferogram is produced to highlight discrepancies between two images, aiding in the analysis of surface movements. 9. Individual burst interferograms are merged to form a map for detailed analysis.10. Coherence data is filtered with Goldstein filter (Goldstein, 1988) to enhance quality by eliminating noise and improving accuracy in the analysis. 11. Phase unwrapping transforms phase data into a surface, facilitating the interpretation of the interferogram. All outcomes of these steps are given in the Results section.

The ascending and descending orbit data were processed separately using ISCE2 software with 5 neighbor connections, resulting in 1605 interferograms from ascending data and 1860 from descending data.

In addition to its main goal that is determining spati-temporal deformation in Düzce region, this study also investigated the Mw6.0 Düzce earthquake that occurred on November 23, 2022. Sentinel-1 ascending and descending data were used to create interferograms. The interferograms were made using the topsApp tool in ISCE2 software specially designed for handling Sentinel-1 Terrain Observation by Progressive Scans (TOPS) data. Since the area of interest remained unchanged in time-series and co-seismic studies studies, the existing DEM files were used, eliminating the need to download DEM data.

During processing, the Enhanced Spectral Diversity (ESD) method was utilized

for coregistration to improve the alignment accuracy of radar images and ensure quality outcomes. Statistical Cost Network Flow Algorithm for Phase Unwrapping (SNAPHU) was employed for phase unwrapping to resolve phase ambiguities and produce displacement maps.

Analysis of both ascending and descending Sentinel-1 datasets provided an examination of ground deformation following the Mw6.0 earthquake. The combination of these datasets offered a reliable understanding of the seismic event, providing valuable insights into fault dynamics and deformation patterns in the Düzce region. This detailed interferometric analysis, given in the Results part, is essential for evaluating the effects of the earthquake and comprehending tectonic activity in the area.

4.3. Velocity Calculation with SBAS

Throughout our processing, we noted a ramp effect caused by errors. To address this issue, we implemented a linear deramping procedure in MintPY to effectively eliminate the trend from the interferograms, resulting in precise velocity maps.

We encountered a data gap in our Sentinel-1 dataset between 2015 and 2017, significantly impacting the coherence and overall results. To mitigate the effects of this gap, we decided to start our analysis on June 2, 2017, and extend it to include interferograms up to the November 23, 2022, Düzce earthquake. By focusing on this continuous period, we aimed to enhance the consistency and accuracy of our velocity calculations.

In order to correct for atmospheric effects, we applied tropospheric corrections using ERA5 data. This correction is of paramount importance as atmospheric delays can distort the phase information in the SAR images, leading to inaccuracies in the measured ground deformation. By applying corrections and utilizing the SBAS method during interferogram processing, we produced velocity maps for the Düzce region.

5. Results

5.1. InSAR Time Series Analysis

In this research, the study focused on time series analysis of InSAR data to understand the ground deformation rate over time in the Düzce region, along the North Anatolian Fault Zone (NAFZ). Using Sentinel-1 data from 2017 to 2022, detailed interferogram networks were processed with the Small Baseline Subset (SBAS) method to track surface displacement changes. These interferograms, connected with five neighboring scenes to improve data quality, capture seismic events and provide a comprehensive picture of ground deformation. The study utilized ascending and descending interferogram networks depicted in Figure 5.1 and Figure 5.2, respectively. Each Synthetic Aperture Radar (SAR) scene was linked to its five neighbors to obtain in a set of interferograms. The ascending dataset covered the period from June 2, 2017 to October 10, 2022 while the descending dataset spanned June 2, 2017 to October 4, 2022. This network setup facilitated generating five interferograms per SAR scene for analysis of deformation patterns.

The assessment of InSAR data quality relied heavily on geocoded spatial coherence and temporal coherence measures. Figure 5.3 displays the geocoded average spatial coherence map for the ascending data. The map highlights the high levels of coherence in sparsely vegetated areas of the NAFZ. Moreover the northern part of the region, including cities such as Sakarya, Düzce and Bolu, also shows coherence. However, forested areas such as the Almacık Block exhibited lower coherence due to limitations of the C band radars ability to penetrate. In Figure 5.4 you can see a map showing the temporal coherence for ascending data. It demonstrates that the southern part of the NAFZ has low coherence while the northern part around urban areas maintained higher levels of coherence.

When looking at the descending data in Figure 5.5 displaying spatial coherence

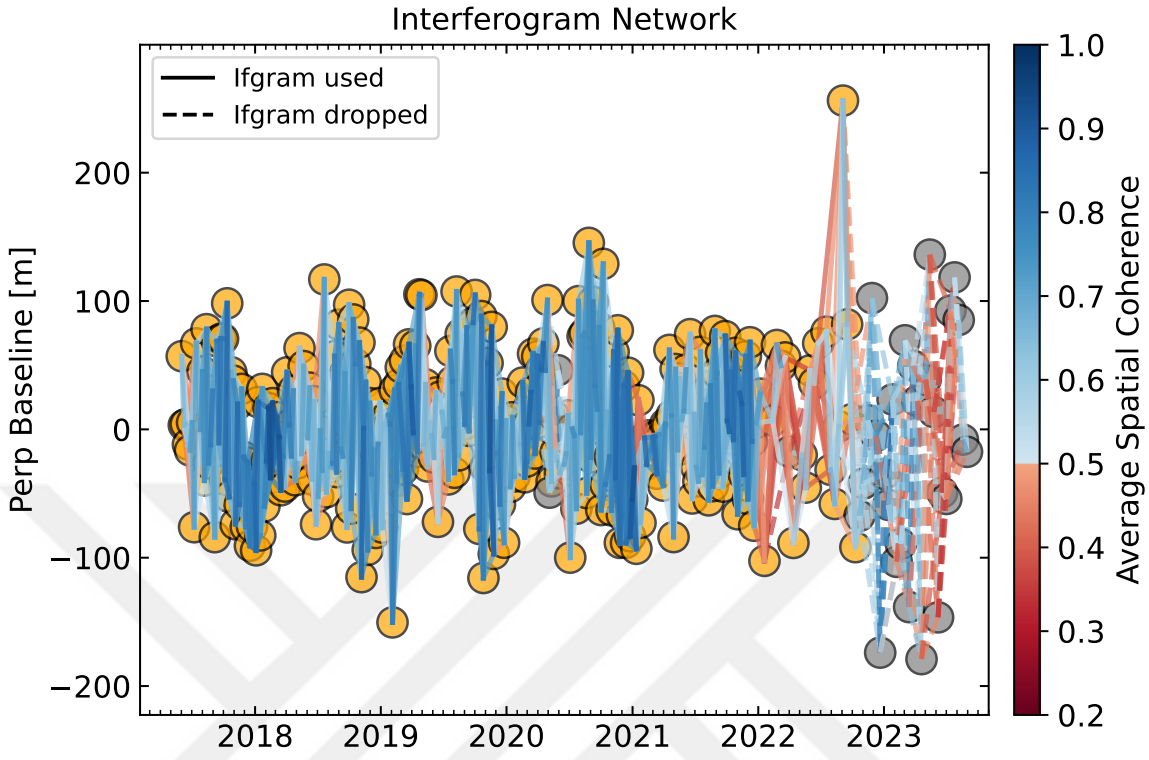

Figure 5.1. Interferogram network of ascending orbit SLCs used. Continuous line represents the used interferograms and the dashed line represents the extracted interferograms. Data from October 10 2022 to 2023 are excluded. Cold colors represent the high coherence between SLC pairs and warm colors represent the low coherence between SLC pairs.

maps, we notice that despite the lower coherence compared to the ascending data there is still higher coherence in the south of the NAFZ with urban areas showing higher values than their surroundings. Figure 5.6 showing geocoded coherence for descending data reveals a contrast with ascending data; there's actually higher coherence south of the NAFZ and significantly lower coherence in the north. This discrepancy highlights how diverse surface and atmospheric conditions in this region can impact InSAR measurements.

A velocity model created using Mintpy software provides an overview ground displacement rates. Figures 5.7 and Figure 5.8 are velocity models for both ascending and descending datasets without any masking applied. In the data analysis we noticed

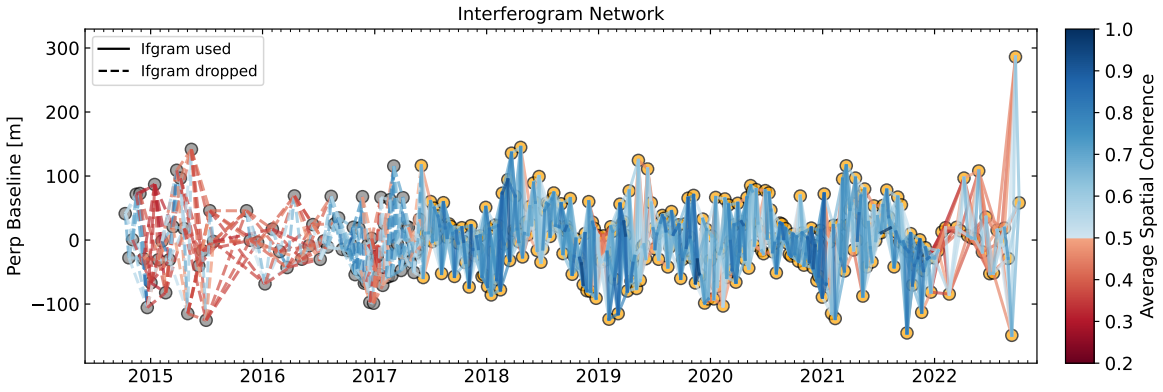

Figure 5.2. Interferogram network of descending orbit SLCs used. Continuous line represents the used interferograms and the dashed line represents the dropped interferograms. Data from 2014 to 02.06.2017 are excluded. Cold colors represent the high coherence between SLC pairs and warm colors represent the low coherence between SLC pairs.

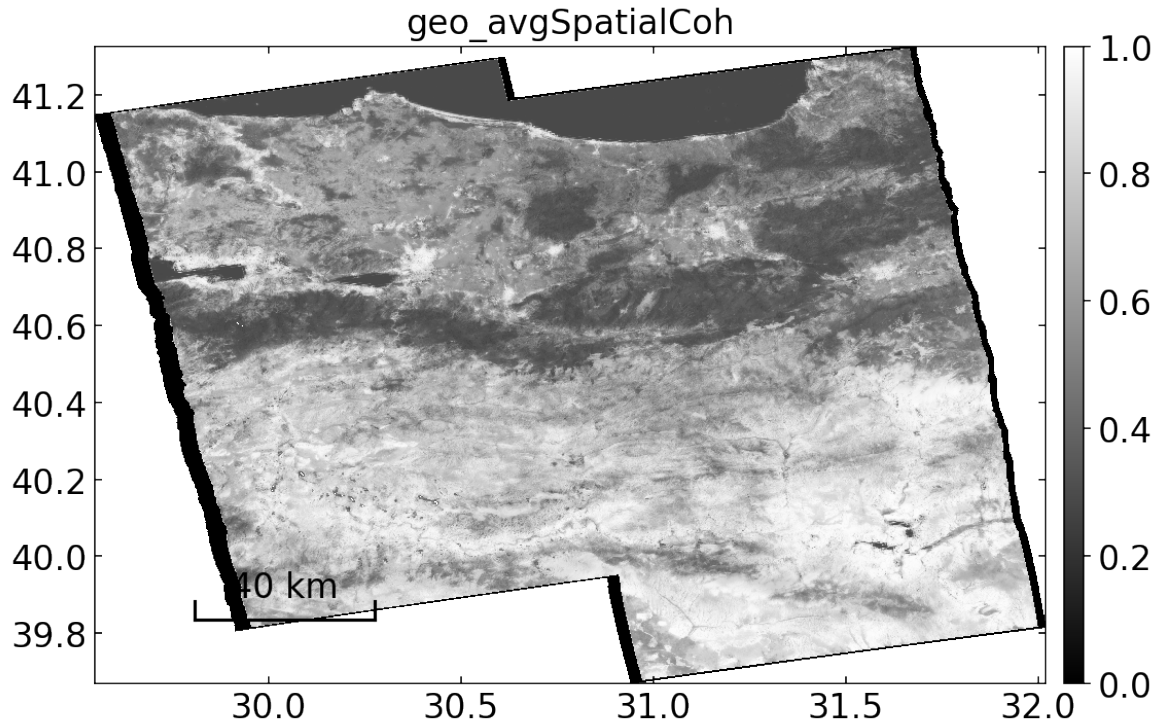

Figure 5.3. Geocoded average spatial coherence of ascending data. Bright colors represent high coherence and the dim colors represent low coherence.

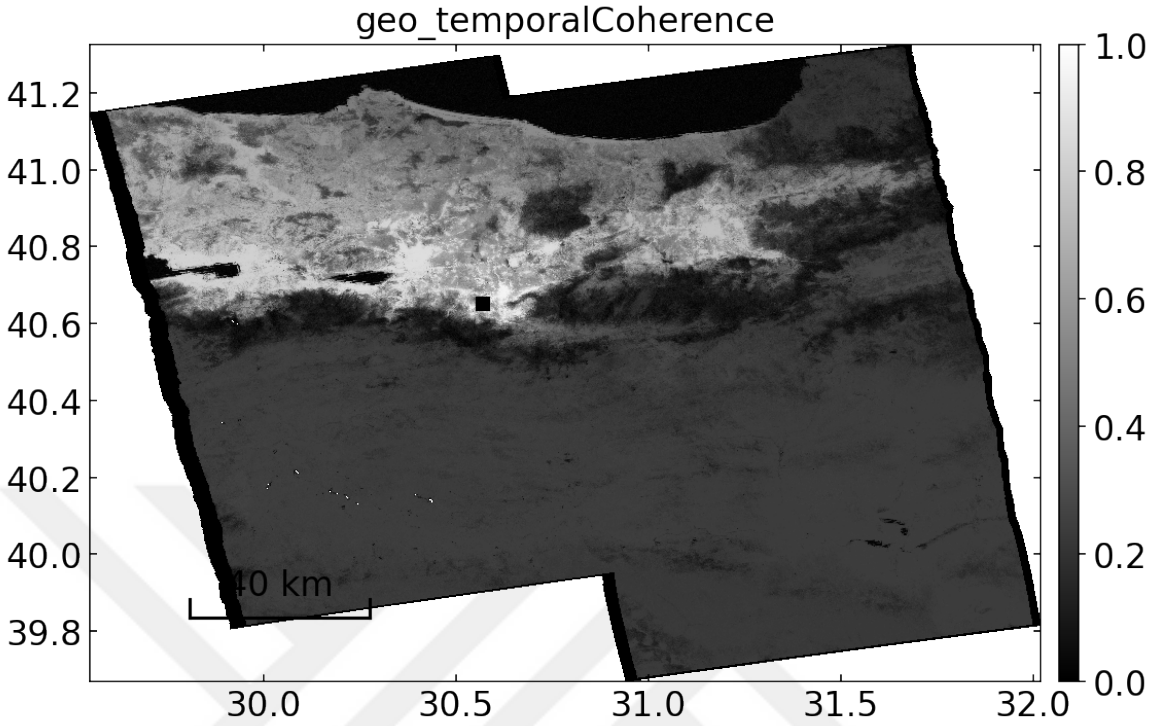

Figure 5.4. Geocoded temporal coherence of ascending data. Bright colors represent areas of high coherence and dim colors represent areas of low coherence.

two areas with very slow velocities, to the south and southeast of the NAFZ, which made it hard to see the overall trend clearly. When we checked the location of these areas, we found out that they were indeed mining sites. In order to enhance the visibility of the NAFZ pattern, we adjusted the velocity range in our figure, setting it between -3 and 3 cm/year. This adjustment revealed the outline of the NAFZ. The final model (Figure 5.9.) indicates that the Anatolian block situated to the south of the fault is undergoing a westward movement at a rate of approximately 2.5 to 3 centimeters per year.

When analyzing the data we chose a reference point north of the NAFZ to be consistent with our findings on ascending data, considering its high coherence and proximity to the fault. Figure 5.10. illustrates an adjusted descending velocity model from 02.06.2017, showing movement patterns as observed in ascending data. The Anatolian block is shown to be moving from the reference point at rates comparable to those observed in the ascending data. The northern part of this model may be affected

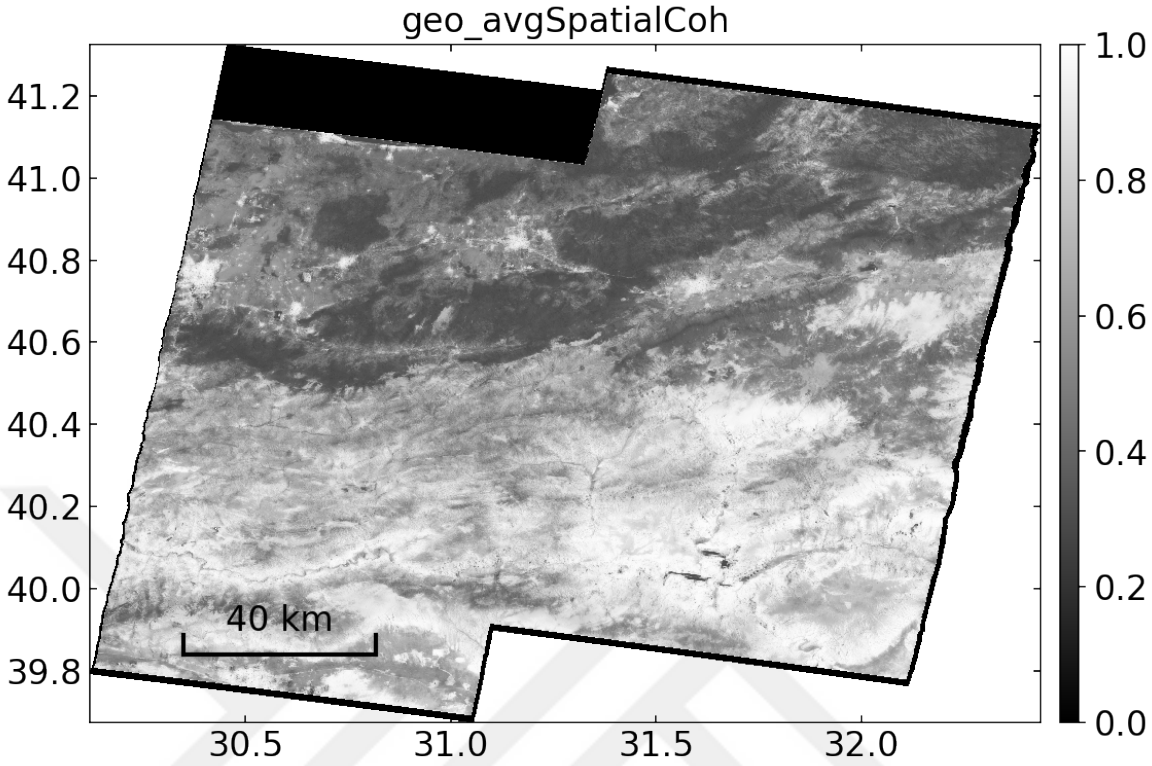

Figure 5.5. Geocoded average spatial coherence of descending data. Bright colors represent areas of high coherence and dim colors represent areas of low coherence.

by edge effects and unwrapping errors indicated by areas on it. The descending model also confirms a block movement with an average rate of about 2.5 - 3 cm/year.

Our comprehensive InSAR studies provide an insight into the deformation patterns that indicate ground displacement in the Düzce region and identify potential seismic hazard zones.

5.2. InSAR Co-seismic Analysis of 23 November 2022 Mw6.0 Gölyaka (Düzce) Earthquake

According to the Boğaziçi University Kandilli Observatory and Earthquake Research Institute (KOERI), a notable earthquake with a moment magnitude of Mw 6.0 occurred on November 23, 2022, at 04:08 local time. The earthquake was located in the Sarıdere-Gölyaka-Düzce region at coordinates 40.8175°N, 30.9868°E. The earthquake

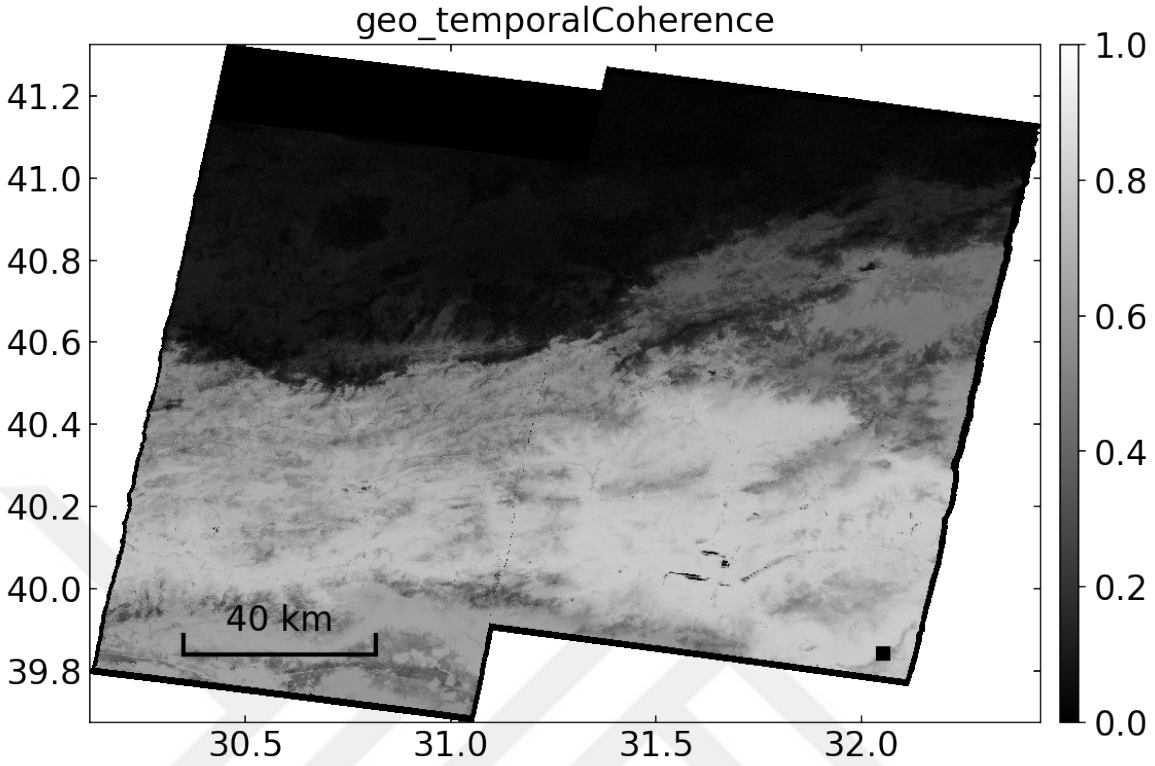

Figure 5.6. Geocoded temporal coherence of descending data. Bright colors represent areas of high coherence and dim colors represent areas of low coherence.

took place at a shallow depth of around 10.6 km, and the fault displayed strike-slip characteristics. The fault characteristics were determined to have a strike of 77°, a dip of 65°, and a rake of -168° (AFAD), demonstrating the intricate nature of the seismic event. In order to examine this occurrence, the Sentinel-1 SLC data was analyzed using ISCE2 software, both in ascending and descending order. The ascending track utilized data from November 15, 2022, and November 27, 2022, whereas the descending track employed data from November 14, 2022, and November 26, 2022. The coherence threshold for Enhanced Spectral Diversity (ESD) was set to 0.8 for both tracks, employing a filter strength of 0.7 for ascending data and 0.5 for descending data to guarantee optimal visibility of the interferogram.

The geocoded coherence maps offer valuable information regarding the quality and reliability of the data. Figure 5.11 displays the geocoded coherence map derived from the ascending data, indicating significant coherence values (about 0.8 – 1.0) over

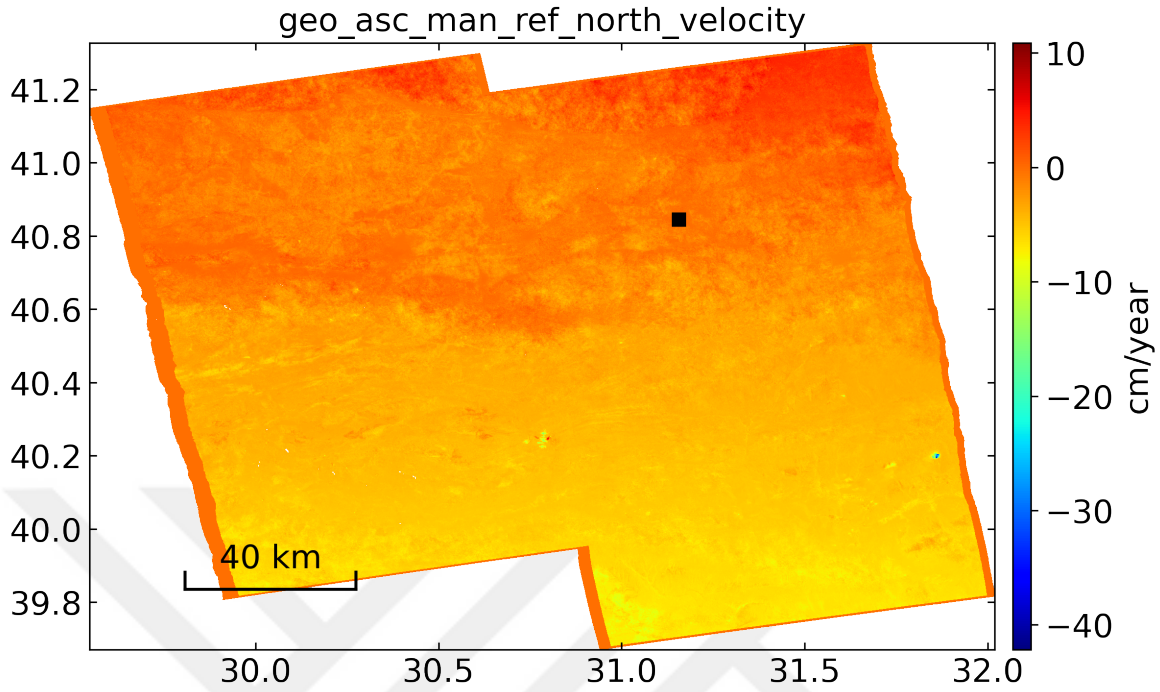

Figure 5.7. Unmasked velocity map obtained from MintPY with using ascending SLCs. Warm colors represent the positive velocities (motion towards the reference point.) and the cold colors represent the negative velocities (motion away from the reference point).

most of the majority of the area, with the exception of the Almacık Block and Sakarya Basin. The strong coherence observed in these locations is indicative of the reliable quality of the data. In contrast, Figure 5.12 displays the geocoded coherence map of the descending data, indicating significantly lower coherence values (0.1 – 0.2) over the region. As a result, the wrapped and unwrapped interferograms derived from this data are considered less trustworthy.

The filtered geocoded wrapped interferogram obtained from the ascending data (Figure 5.13) clearly displays the earthquake anomaly at the epicenter. The anomaly appears as a circular pattern, deviating from the usual butterfly form, which suggests a prominent normal faulting component. The filtered geocoded unwrapped interferogram (Figure 5.14), which exhibits strong coherence, plainly illustrates the effects of the earthquake. The Almacık Block is characterized as the most noisy area due to its complex topography and high vegetation. Due to the high reliabilty of the ascend-

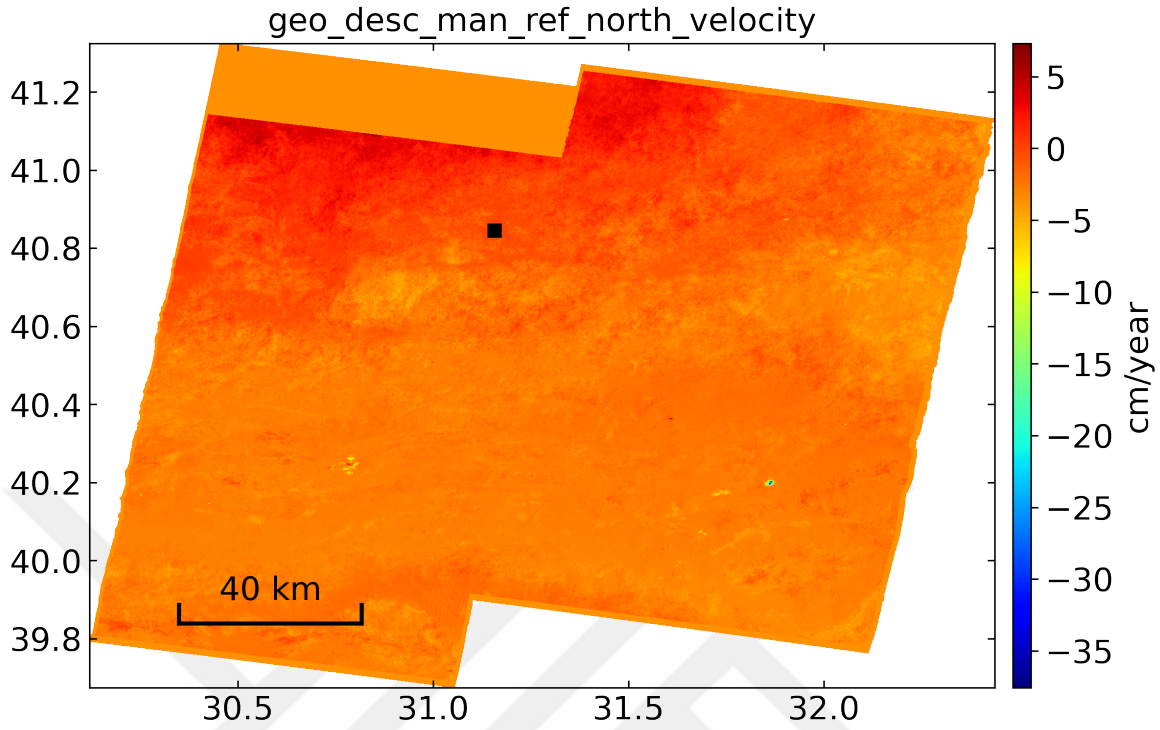

Figure 5.8. Unmasked velocity map obtained from MintPY with using descending SLCs. Warm colors represent the positive velocities (motion through the reference point.) and the cold colors represent the negative velocities (motion away from the reference point).

ing interferogram, we performed GACOS atmospheric correction and afterwards, we masked with coherence map with 0.4 threshold. This resulted in a cleaned figure where noise in the Almacık Block was well concealed as shown in Figure 5.15.

On the other hand, the filtered geocoded wrapped interferogram that is descending in nature (as shown in Figure 5.16) displays extensive noise that is not limited to the Almacık Block but impacts the entire dataset, hence diminishing its reliability. The earthquake's epicenter is clearly discernible in the upper-right part of the interferogram. The geocoded unwrapped interferogram shown in Figure 5.17, after filtering, does not exhibit any visually visible anomaly associated with the earthquake. This suggests that this particular interferogram cannot be reliably utilized in subsequent processes, such as slip modeling.

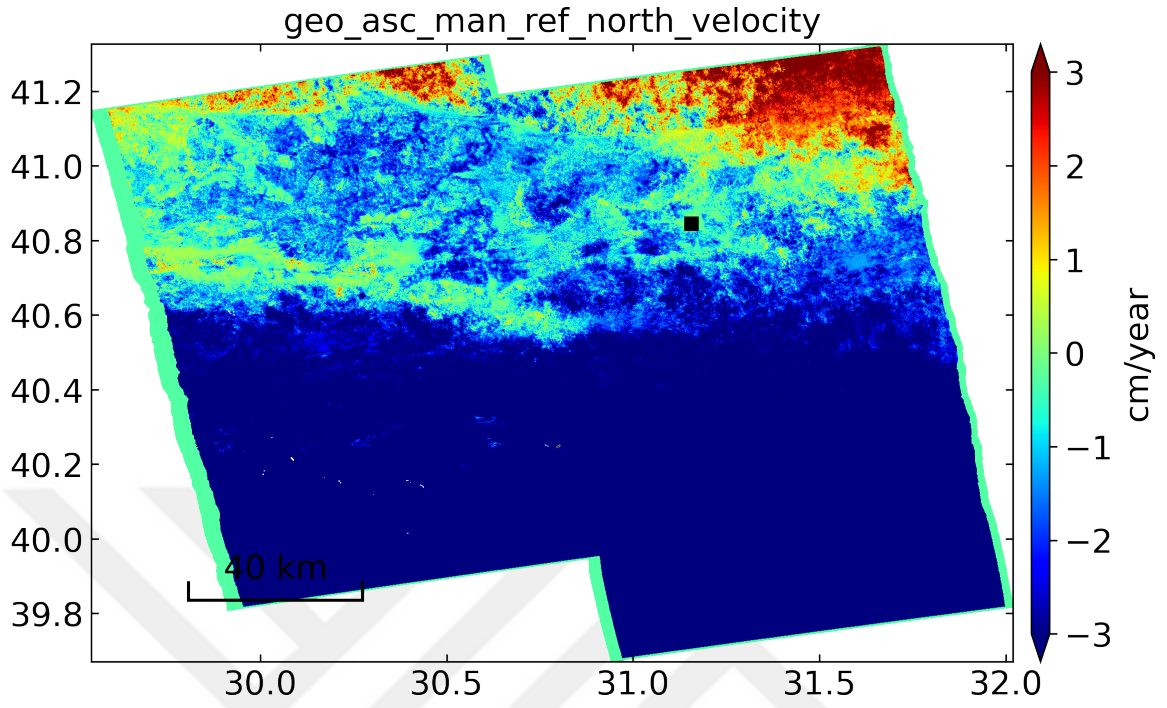

Figure 5.9. Adjusted velocity map between -3 cm/ year and 3 cm/year obtained from MintPY with using ascending SLCs. Warm colors represent the positive velocities (motion through the reference point.) and the cold colors represent the negative velocities (motion away from the reference point).

Because of the lack of consistency and resulting lack of reliability, no modifications were made to the descending data to account for atmospheric conditions or to remove unwanted data.

The meticulous examinations underscore the notable discrepancies in data integrity between ascending and descending paths, underscoring the significance of choosing appropriate data and parameters for InSAR processing to fully capture the impact of seismic events.

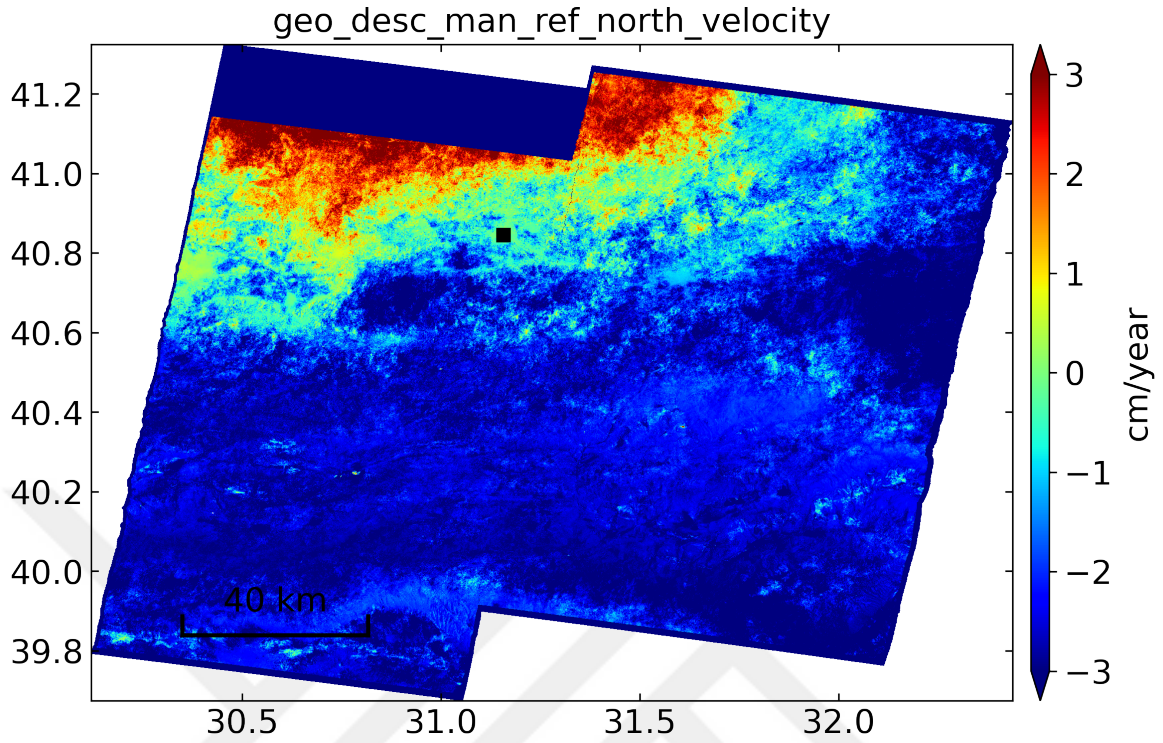

Figure 5.10. Adjusted velocity map between -3 cm/ year and 3 cm/year obtained from MintPY with using descending SLCs. Warm colors represent the positive velocities (motion through the reference point.) and the cold colors represent the negative velocities (motion away from the reference point).

5.3. Coulomb Stress Analysis of 23 November 2022 Mw6.0 Gölyaka (Düzce) Earthquake

The Coulomb stress analysis of the Mw6.0 Gölyaka (Düzce) earthquake on 23 November 2022 offers valuable information on the alterations in stress distribution caused by this seismic event. The earthquake's parameters were determined by AFAD are given as follows: a depth of 6.81 km, a strike angle of 77°, a dip angle of 65°, a rake angle of −168°, and we took the friction coefficient as 0.4. Figure 5.18 depicts the Coulomb stress fluctuations, with cold colors indicating stress reduction and warm colors representing stress accumulation. The investigation indicates a decrease in stress in the western and eastern sections of the Düzce Fault, but there was a considerable increase in stress in the southern segment of the fault. Similarly, the western and eastern sections of the NAF in the vicinity underwent stress reduction, whereas the

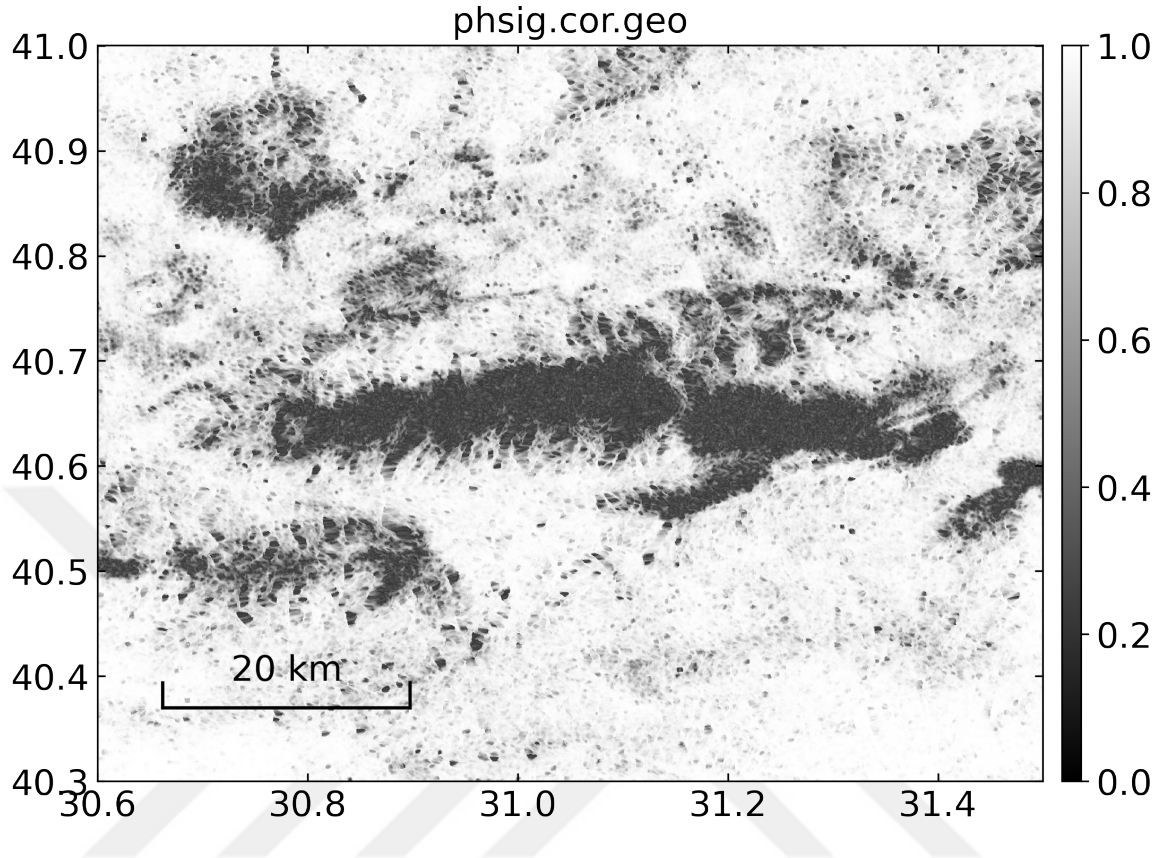

Figure 5.11. The coherence map of ascending interferogram obtained from ISCE2. Bright colors represent the high coherence and the dim colors represent the low coherence.

southern sections increased tension. In addition, stress building was seen in both the western segment of the Hendek Fault and the eastern segment, which is located near the earthquake site. The northern section of the NAF, which runs through İzmit, also experienced elevated levels of stress.

Figure 5.19 displays the Coulomb stress analysis of the mainshock and subsequent aftershocks. This study utilizes the earthquake catalog and focal mechanism solutions provided by AFAD shown in Table 5.1, assuming a friction coefficient of 0.4. According to this analysis, the occurrence of aftershocks caused the build-up of stress in the eastern section of the Düzce Fault, as well as in both the western and eastern parts of the NAF. The northern segment of the Hendek Fault likewise underwent stress accumulation, but its eastern continuation underwent stress reduction. Likewise, there

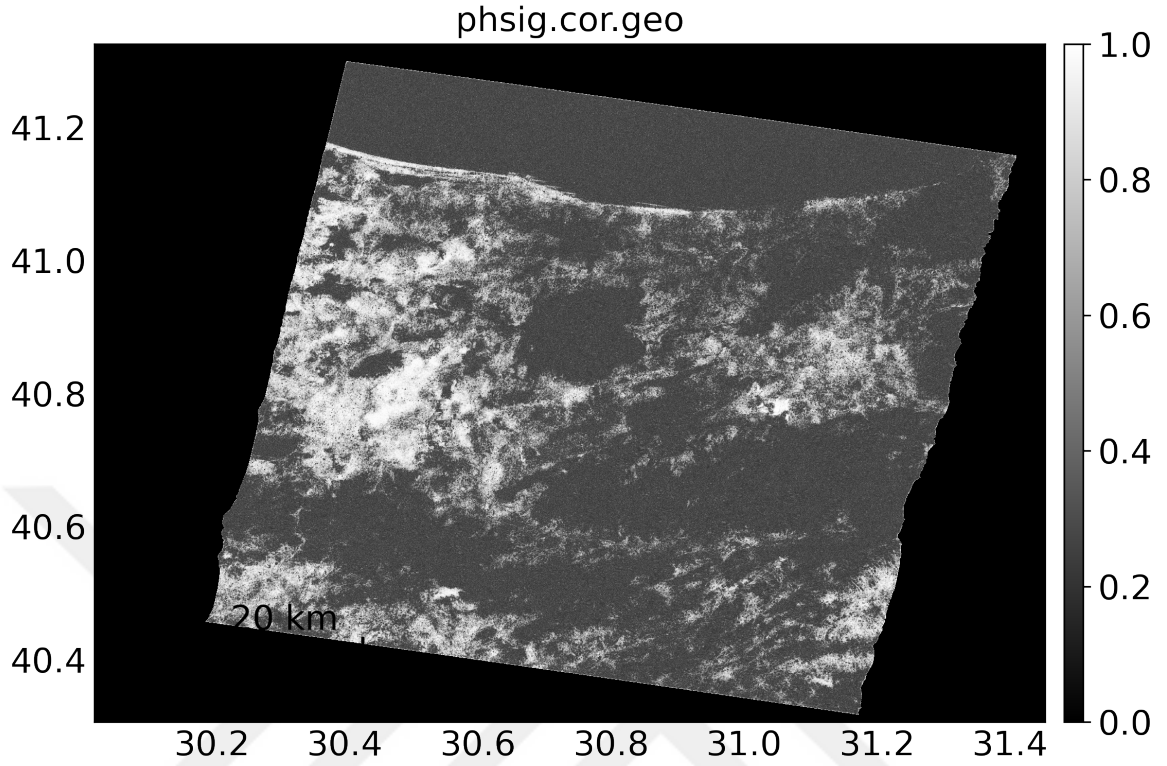

Figure 5.12. The coherence map of descending interferogram obtained from ISCE2. Bright colors represent the high coherence and the dim colors represent the low coherence.

was a notable decrease in tension seen in the western section of the Düzce Fault.

Date	Latitude	Longitude	Depth	Magnitude	Location	Strike1	Dip1	Rake1	Strike2	Dip2	Rake2
2023-10-14T14:07:09	40.874	31.736	7.7	4.5	Merkez (Bolu)	281	74	-156	184	67	-17
2023-03-16T10:55:06	40.792	31.525	9.12	4.8	Merkez (Bolu)	206	78	-10	299	80	-168
2022-11-23T03:50:58	40.789	30.957	9.45	4.3	Merkez (Bolu)	254	83	177	345	87	7
2022-11-23T01:08:15	40.823	31.025	6.81	5.9	Merkez (Bolu)	77	65	-168	342	79	-26

Table 5.1. Earthquake catalog and fault parameters obtained from AFAD

In the third study, specifically in Figure 5.20, we conducted a Coulomb stress analysis for the mainshock and aftershocks (see Table 5.1). The depth was not fixed and was allowed to vary between 0 and 15 km. Throughout the analysis, a friction coefficient of 0.4 was maintained. This methodology yielded a more comprehensive depiction of stress transmission and buildup. The findings suggest that a substantial amount of energy was transmitted to the Düzce Fault, particularly to the eastern segment. In addition, the NAF exhibited a higher level of stress buildup following the incident and subsequent aftershocks. The analysis also indicates that the western

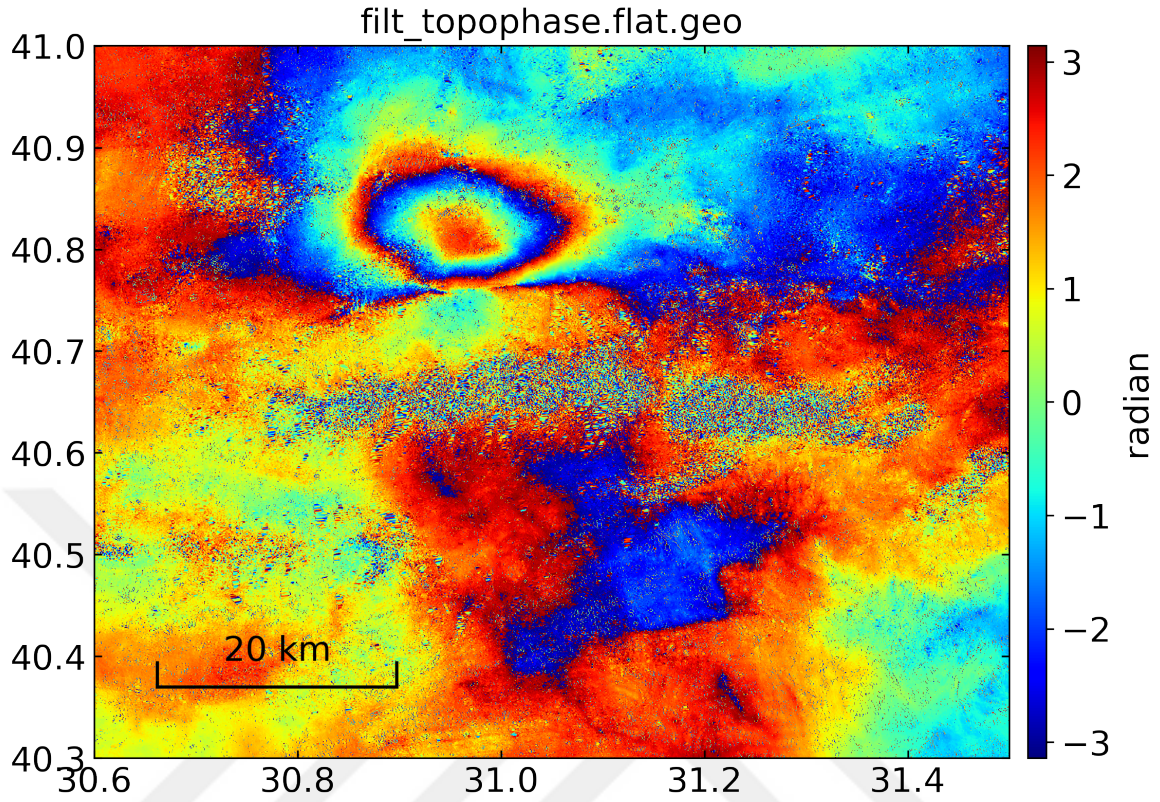

Figure 5.13. Wrapped interferogram obtained by using ascending orbit SLCs.

portion of the Düzce Fault and the eastern portion of the Hendek Fault underwent stress relief.

These findings highlight the intricate interplay among different fault segments in the region subsequent to the Mw6.0 Düzce earthquake. The comprehensive analysis of Coulomb stress variations offers essential insights into the prediction of future earthquake risks and the development of efficient solutions for risk mitigation efforts.

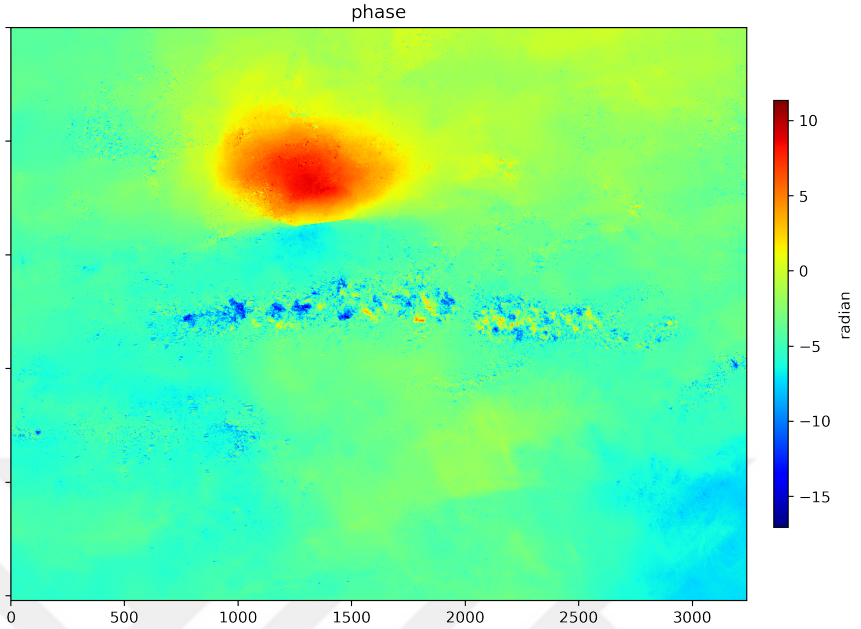

Figure 5.14. Unwrapped interferogram obtained by using ascending orbit SLCs. Warm colors represent the motion away from the satellite and the cold colors represent the motion towards the satellite.

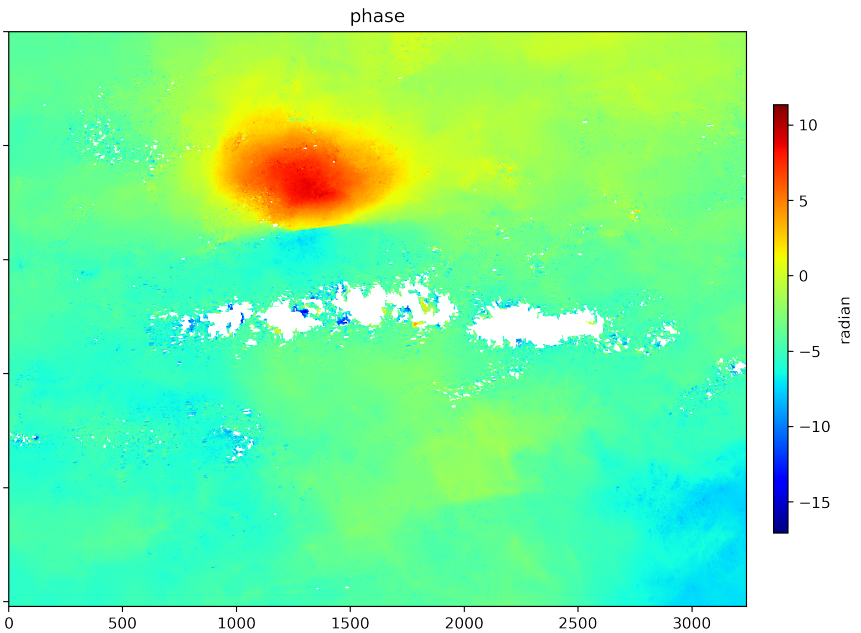

Figure 5.15. Unwrapped masked interferogram masked with coherence file, obtained by using ascending orbit SLCs. Warm colors represent the motion away from the satellite and the cold colors represent the motion towards the satellite.

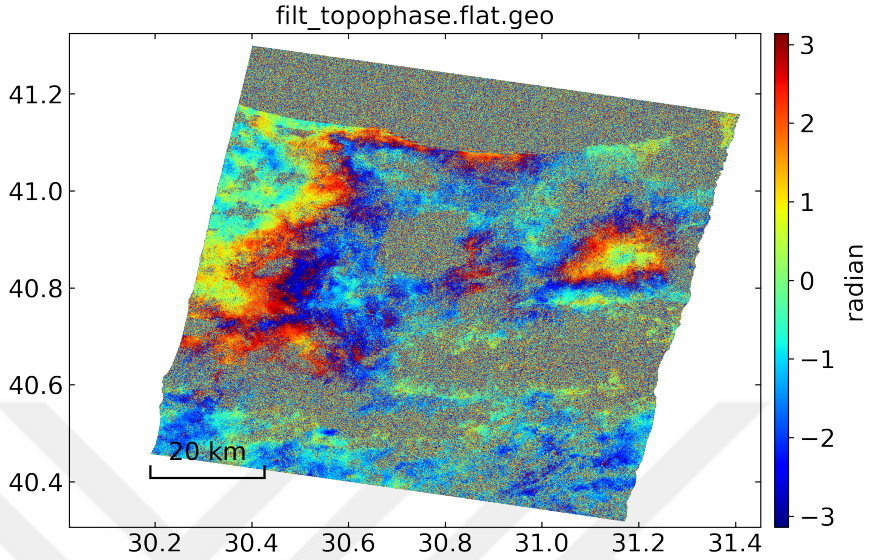

Figure 5.16. Wrapped interferogram obtained by using descending orbit SLCs.

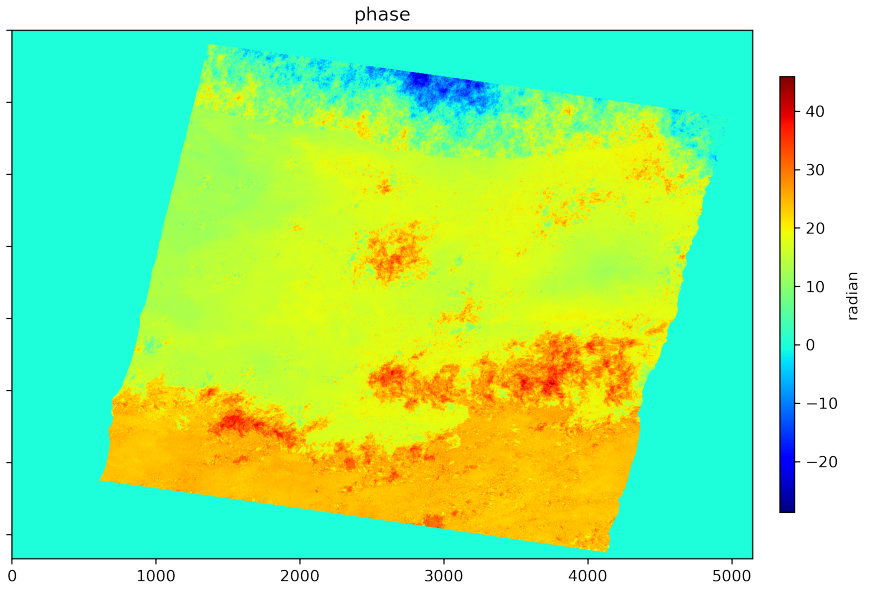

Figure 5.17. Unwrapped interferogram obtained by using descending orbit SLCs. Warm colors represent the motion away from the satellite and the cold colors represent the motion towards the satellite.

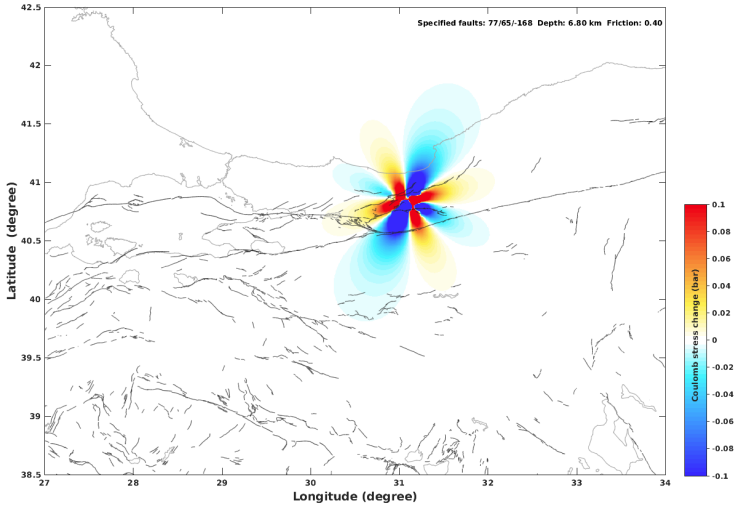

Figure 5.18. Coulomb stress analysis of 23 November 2022 Düzce earthquake. Warm colors represent the stress buildup and the cold colors represent the stress relief. 77° of strike, 65° of dip and −168° of rake is used as fochal mechanism solution parameters (Obtained from AFAD). Depth is 6.81 km and friction coefficient is 0.4.

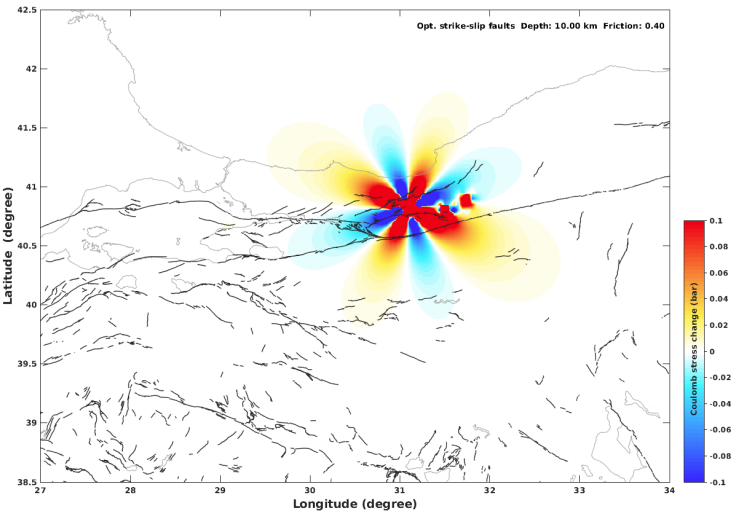

Figure 5.19. Coulomb stress analysis of 23 November 2022 Düzce earthquake with aftershocks. 77 degrees of strike, 65 degrees of dip and -168 degrees of rake is used for the mainshock as focal mechainsm solution parameters (Obtained from AFAD). Depth is fixed to 10 km and friction coefficient is 0.4.

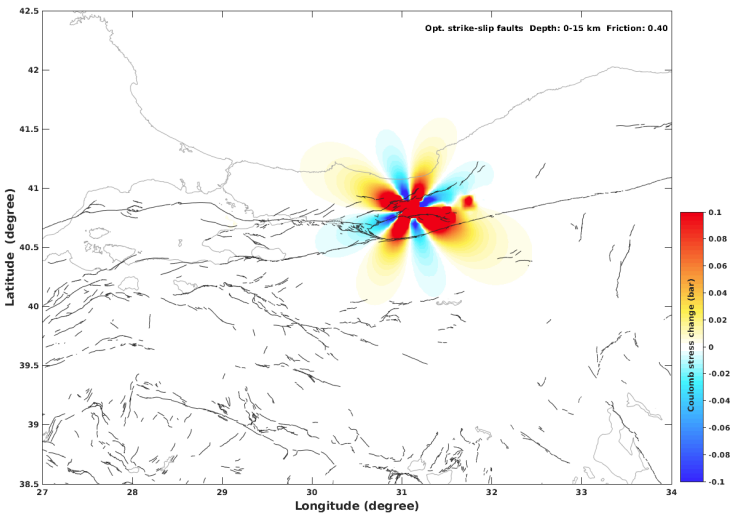

Figure 5.20. 77 degrees of strike, 65 degrees of dip and -168 degrees of rake is used as fochal mechainsm solution parameters (Obtained from AFAD. Depth is ranged from 0 to 15 km and friction coefficient is 0.4.

6. Discussion & Conclusion

The findings of this thesis offer valuable insights into the seismic behavior and structural properties of the Düzce region and the North Anatolian Fault Zone (NAFZ). By employing Interferometric Synthetic Aperture Radar (InSAR) time series and co-seismic analyses, coupled with Coulomb stress modelling, we have obtained crucial insights into the patterns of ground deformation and the accumulation of stress along this fault system that is highly active in terms of tectonic activity.

The Line of Sight (LOS) velocity obtained for the Düzce region in this study is approximately $25 - 30$ mm/year, which is comparable to the velocities obtained from previous geodetic studies (Hussain et al., 2018). The ongoing accumulation of seismic energy in the region has caused a displacement of $\sim$ 40 mm with the 2022 Düzce earthquake.

6.1. Comparison with Seismic Tomography and Magnetotelluric Surveys

The pattern of deformation can be deduced using geodetic information, seismic activity, and seismic anisotropy. Geodetic data, such as Insar and GPS measurements, offer insights into the present-day deformation of the Earth's upper crust. Meanwhile, seismic anisotropy reflects both historical and ongoing deformation. Wang et al. (2020) utilized three dimensional seismic tomography to examine the P-wave velocity (Vp) and seismic anisotropy in the crust and uppermost mantle beneath Türkiye. Their research revealed notable variations in seismic velocities and anisotropy in the vicinity of the Düzce region indicating complex tectonic interactions and the existence of zones that are saturated with fluids and fractured rock. The general seismic velocity pattern of the NAFZ in the wesrtern Düzce region indicates low-velocity zones, which suggest potential weak areas along the fault, while these velocities increase towards the east and north. This could imply that the western part of the Düzce region was more deformed in the past comparing to the eastern part and was able to accumulate less

strain with less deformation casuing smaller earthquakes.

Magnetotelluric (MT) investigations, conducted by Kaya et al., (2009) have investigated the resistivity distribution in the region and detected areas of high electrical conductivity south of the Düzce Fault suggesting the existence of fluids within fault zones. These fluids can facilitate seismic slip by reducing the friction of faults and may be the reason of the higher slip values observed south of the Düzce fault or affect the occurrence of seismic events. Our InSAR time series analysis results reveal the complex structure of the Düzce region and show lower slip values in the eastern parts where MT results indicate the presence of a more resistive structure in the same region. This indicate that the results obtained by MT method are consistent with the surface deformation observed through the InSAR method, emphasizing the influence of fluids on the fault mechanics.

6.2. Implications for Seismic Hazard Assessment

An understanding of surface deformation in the Düzce region is of paramount importance for the assessment of seismic threat. Deformation patterns indicate the presence of regions exhibiting stress accumulation, which is associated with an elevated seismic risk. By integrating InSAR time series data with seismic tomography and MT results, it is possible to identify areas that could potentially impact seismic activity.

Toda et al. (2005) employed Coulomb stress analysis to examine the impact of the 1999 Izmit and Düzce earthquakes on stress levels. Their research findings indicated the existence of areas currently experiencing elevated stress levels, particularly those situated to the east and west of the Düzce fault, as well as some sections of the North Anatolian Fault (NAF) system. It is probable that these areas will experience a greater frequency of earthquakes in the future as a consequence of the transfer of stress from the aforementioned major seismic events. A comparison of these data with the stress variations observed in the 2022 Mw 6.0 Düzce earthquake will facilitate an enhanced comprehension of the developing seismic risk in the area. The 2022 earth-

quake primarily increased stress along the southern section of the Düzce fault and the northern segments of the NAF, which may potentially result in future seismic activity in these regions.

The identification of regions exhibiting high and low deformation is of paramount importance for the assessment of seismic hazards. Locked segments are capable of accumulating significant stress and frequently experience large earthquake events, underscoring the necessity for detailed analysis. By integrating our InSAR observations with seismic tomography and MT analysis, we are able to accurately identify these areas of high roughness, thereby providing crucial information for earthquake preparedness and risk mitigation.

6.3. Conclusion

In this thesis, we employed InSAR time series analysis, utilizing Sentinel-1 data spanning from 2014 to 2022. Our goal was to examine surface deformation and investigate how crustal properties relate to fault mechanics in the Düzce segment of the NAFZ. The LOS velocity determined for the Düzce region in this research is approximately 25-30 mm/year, which is consistent with the velocities reported in earlier geodetic investigations. In addition to studying long-term deformation in the Düzce region, we also investigated the effects of the 2022 Mw6.0 Gölyaka-Düzce earthquake by comparing deformation before and after the event using both ascending and descending InSAR datasets. The continuous accumulation of seismic energy in the area has led to a displacement of about 40 mm during the 2022 Düzce earthquake. The integration of InSAR time series analysis with seismic tomography and magnetotelluric surveys offers a comprehensive understanding of geophysical phenomena and seismic risks in the Düzce region. The conjunction of surface deformation patterns, velocity structures, and the distribution of fluids in the subsurface indicates locations of elevated seismic risk. A comprehension of these deformation patterns is imperative for the development of effective methodologies for the assessment of seismic risk and the mitigation of its effects. The 2022 Mw6.0 Düzce earthquake has highlighted the importance of ongoing

monitoring and comprehensive geophysical investigations with regard to the impact on regional stress distribution. These efforts are crucial for advancing our comprehension of fault dynamics and enhancing earthquake preparedness.

REFERENCES

Akyüz, H. S., Hartleb, R., Barka, A. A., Altunel, E., Sunal, G., Meyer, B., & Armijo, R., "Surface Rupture and Slip Distribution Along the 17 August 1999 İzmit Earthquake (M 7.4) North Anatolian Fault, Turkey", *Bulletin of the Seismological Society of America*, 92(1), 61-66, 2002.

Ambraseys, N., & Jackson, J., "Seismicity of the Sea of Marmara (Turkey) Since 1500", *Geophysical Journal International*, 141(3), F1-F6, 2000.

Anderlini, L., *Kinematic models of interseismic deformation from inversion of GPS and InSAR measurements to estimate fault parameters and coupling degree* (Doctoral dissertation, Alma Mater Studiorum – Università di Bologna), 2014.

Armijo, R., Meyer, B., Hubert, A., & Barka, A., "Westward propagation of the North Anatolian fault into the northern Aegean: Timing and kinematics", *Geology, 27*(3), 267-270, 1999.

Aslan, G., Ergintav, S., Reilinger, R. E., Floyd, M., Cakmak, R., Lasserre, C., ... & Barka, A. A., "Shallow Creep Along the 1999 İzmit Earthquake Rupture, Turkey, From GPS and High Temporal Resolution InSAR", *Journal of Geophysical Research: Solid Earth*, 124(5), 4917-4934, 2019.

Bamler, R., & Hartl, P., "Synthetic Aperture Radar Interferometry", *Inverse Problems*, 14*(4), R1-R54, 1998.

Barış, Ş., Nakajima, J., Hasegawa, A., Honkura, Y., Ito, A., & Üçer, S.B., "Three-dimensional Structure of Vp, Vs and Vp/Vs in the Upper Crust of the Marmara Region, NW Turkey", *Earth Planets Space*, 57, 1019-1038, 2005.

Barka, A. A., "Slip Distribution Along the North Anatolian Fault Associated with the Large Earthquakes of the Period 1939 to 1967", *Bulletin of the Seismological Society of America*, 86(5), 1238-1254, 1996.

Barka, A. A., "The 17 August 1999 İzmit Earthquake", *Science*, 285(5435), 1858-1859, 1999.

Berardino, P., Fornaro, G., Lanari, R., & Sansosti, E., "A New Algorithm for Surface Deformation Monitoring Based on Small Baseline Differential SAR Interferograms", *IEEE Transactions on Geoscience and Remote Sensing*, 40(11), 2375-2383, 2002.

Birgoren, G., Sekiguchi, H., & Irikura, K., "Rupture Model of the 1999 Duzce, Turkey, Earthquake Deduced from High and Low Frequency Strong Motion Data", *Geophysical Research Letters*, 31, L05610, 2004.

Bletery, Q., Sladen, A., Jiang, J., Simons, M., Owens, M., & Ampuero, J. P., "A Bayesian Source Model for the 2004 Great Sumatra-Andaman Earthquake", *Journal of Geophysical Research: Solid Earth*, 121(8), 5116-5135, 2016.

Bletery, Q., Thomas, A. M., Rempel, A. W., Karlstrom, L., Sladen, A., & De Barros, L., "Fault Curvature and Earthquake Rupture Dynamics", *Journal of Geophysical Research: Solid Earth*, 124(2), 1671-1687, 2019.

Bohnhoff, M., Martínez-Garzón, P., Bulut, F., Stierle, E., & Ben-Zion, Y., "Maximum Earthquake Magnitudes Along Different Sections of the North Anatolian Fault Zone", *Tectonophysics, 674*, 147-165, 2016.

Bozkurt, E., "Neotectonics of Turkey—a synthesis", *Geodinamica Acta, 14*(1-3), 3-30, 2001.

Bürgmann, R., Ergintav, S., Segall, P., Hearn, E., McClusky, S., Reilinger, R. E.,

... & Cakmak, R., "Time-dependent Distributed Afterslip on and Deep Below the Izmit Earthquake Rupture", *Bulletin of the Seismological Society of America*, 90(6), 1353-1368, 2000.

Bürgmann, R., Rosen, P. A., & Fielding, E. J., "Synthetic Aperture Radar Interferometry to Measure Earth's Surface Topography and Its Deformation", *Annual Review of Earth and Planetary Sciences, 28*, 169-209, 2000.

Bürgmann, R., Kogan, M. G., Steblov, G. M., Hilley, G., Levin, V. E., & Apel, E., "Interseismic Coupling and Asperity Distribution Along the Kamchatka Subduction Zone", *Journal of Geophysical Research: Solid Earth*, 110(B7), 2005.

Cakir, Z., Ergintav, S., & Meghraoui, M., "InSAR Measurements of Postseismic Deformation and Creep Along the Ismetpasa Segment of the North Anatolian Fault (Turkey)", *Geophysical Research Letters, 32*(20), 2005.

Chen, C. W., & Zebker, H. A., "Phase Unwrapping for Large SAR Interferograms: Statistical Segmentation and Generalized Network Models", *IEEE Transactions on Geoscience and Remote Sensing*, 40(8), 1709-1719, 2002.

Colesanti, C., & Wasowski, J., "Investigating Landslides with Space-borne Synthetic Aperture Radar (SAR) Interferometry", *Engineering Geology, 88*(3-4), 173-199, 2006.

Copernicus. (n.d.). *Sentinel-1 SAR Instrument and Acquisition Modes.* Retrieved from https://sentinels.copernicus.eu/en/web/sentinel/technical-guides/sentinel-1-sar/sar-instrument/acquisition-modes.

Crosetto, M., Monserrat, O., Cuevas-González, M., Devanthéry, N., & Crippa, B., "Persistent Scatterer Interferometry: A Review", *ISPRS Journal of Photogrammetry and Remote Sensing*, 115, 78-89, 2016.

Eken, T., Taymaz, T., & Yolsal, S., "Source Mechanisms of Earthquakes in the Eastern Mediterranean Region", *Journal of Seismology*, 17(1), 37-55, 2013.

Emre, O., Duman, T. Y., özalp, S., Şaroğlu, F., & Olgun, Ş., "Active Fault Map of Turkey", *General Directorate of Mineral Research and Exploration, Special Publication Series*, 30, 2013.

Engdahl, E. R., van der Hilst, R., & Buland, R., "Global Teleseismic Earthquake Relocation with Improved Travel Times and Procedures for Depth Determination", *Bulletin of the Seismological Society of America*, 88(3), 722-743, 1998.

England, P. C., Houseman, G. A., and Nocquet, J. M., "Constraints from GPS Measurements on the Dynamics of Deformation in Anatolia and the Aegean", Journal of Geophysical Research: Solid Earth, 2016.

European Space Agency (ESA), *InSAR Principles: Guidelines for SAR Interferometry Processing and Interpretation.* ESA TM-19, Part A. Retrieved from https://www.esa.int/esapub 19_ptA.pdf, 2007.

European Space Agency (ESA), Sentinel-1 SAR Technical Guide: SAR Instrument and Acquisition Modes. Retrieved from https://sentinels.copernicus.eu/en/web/sentinel/technical-guides/sentinel-1-sar/sar-instrument/acquisition-modes, 2013.

Farina, P., Colombo, D., Fumagalli, A., Marks, F., & Moretti, S., "Permanent Scatterers for Landslide Investigations: Outcomes from the ESA-SLAM Project", *Engineering Geology, 88*(3-4), 200-217, 2006.

Fattahi, H., & Amelung, F., "InSAR Uncertainty Due to Orbital Errors", *Geophysical Journal International*, 194(2), 590-595, 2013.

Fattahi, H., & Amelung, F., "InSAR Observation of a Slow Slip Event in the North

Anatolian Fault Zone", Turkey. *Geophysical Research Letters, 41*(10), 3592-3598, 2014.

Fattahi, H., Agram, P., & Simons, M., "A Network-Based Enhanced Spectral Diversity Approach for TOPS Time-Series Analysis" *IEEE Transactions on Geoscience and Remote Sensing*, 55(2), 777-786, 2017.

Ferretti, A., Prati, C., & Rocca, F., "Permanent Scatterers in SAR Interferometry", *IEEE Transactions on Geoscience and Remote Sensing*, 39(1), 8-20, 2001.

Fialko, Y., Sandwell, D., Simons, M., & Rosen, P. A., "Three-Dimensional Deformation Caused by the Bam, Iran, Earthquake and the Origin of Shallow Slip Deficit", *Nature*, 435(7040), 295-299, 2005.

Fialko, Y., Simons, M., & Agnew, D., "The Complete (3-D) Surface Displacement Field in the Epicentral Area of the 1999 M_w7.1 Hector Mine Earthquake, Southern California, from Space Geodetic Observations", *Geophysical Research Letters, 32*(4), 2005.

Fialko, Y., "Interseismic Strain Accumulation and the Earthquake Potential on the Southern San Andreas Fault System", *Nature*, 441(7096), 968-971, 2006.

Gabriel, A. K., Goldstein, R. M., & Zebker, H. A., "Mapping Small Elevation Changes over Large Areas: Differential Radar Interferometry", *Journal of Geophysical Research: Solid Earth*, 94(B7), 9183-9191, 1989.

Geudtner, D., Torres, R., Snoeij, P., Davidson, M., & Rommen, B., "Sentinel-1 System Capabilities and Applications", *European Space Agency Special Publication*, 740, 4, 2014.

Goldstein, R. M., & Werner, C. L., "Radar Interferogram Filtering for Geophysical

Applications", *Geophysical Research Letters*, 25(21), 4035-4038, 1998.

Hansen, P., & Mount, J., "InSAR Data Analysis for Earthquake Monitoring", *Journal of Seismological Research*, 67(3), 227-239, 2013.

Hanssen, R. F., *Radar Interferometry: Data Interpretation and Error Analysis*, Springer Science & Business Media, 2001.

Havazlı, E., et al., "Monitoring Surface Deformation in Tectonically Active Regions Using InSAR and GPS Data", *Journal of Geophysical Research: Solid Earth*, 125(3), e2019JB018192, 2020.

Havazlı, E., Çakır, Z., & Ergintav, S., "Analysis of Postseismic Deformation Following the 2020 Elazığ Earthquake Using Sentinel-1 InSAR Data", *Remote Sensing, 13*(10), 1961, 2021.

Hensley, S., Rosen, P. A., & Gurrola, E., "UAVSAR: An Airborne Synthetic Aperture Radar for Science and Technology Applications. *IEEE Aerospace Conference, 2009*, 1-9, 2009.

Hoffmann, J., Zebker, H. A., Galloway, D. L., & Amelung, F., "Seasonal Subsidence and Rebound in Las Vegas Valley, Nevada, Observed by Synthetic Aperture Radar Interferometry. *Water Resources Research, 39*(9), 2003.

Hooper, A., Zebker, H., Segall, P., & Kampes, B., "A New Method for Measuring Deformation on Volcanoes and Other Natural Terrains Using InSAR Persistent Scatterers", *Geophysical Research Letters, 31*(23), 2004.

Hussain, E., Wright, T. J., Walters, R. J., Bekaert, D., Hooper, A., & Houseman, G. A., "Geodetic Observations of Postseismic Creep in the Decade After the 1999 Izmit Earthquake, Turkey: Implications for a Shallow Slip Deficit", *Journal of Geophysical*

Research: Solid Earth, 121, 2980–3001, 2016.

Hyndman, R. D., & Wang, K., "The Rupture Zone of Cascadia Great Earthquakes from Current Deformation and the Thermal Regime", *Journal of Geophysical Research: Solid Earth*, 100(B11), 22133-22154, 1995.

Jónsson, S., Zebker, H., Segall, P., & Amelung, F., "Fault Slip Distribution of the 1999 Mw7.1 Hector Mine Earthquake, California, Estimated from Satellite Radar and GPS Measurements", *Bulletin of the Seismological Society of America, 92*(4), 1377-1389, 2002.

Kanamori, H. and Anderson, D.L., "Theoretical Basis of Some Empirical Relations in Seismology", *Bulletin of the Seismological Society of America*, 65, 1073-1095, 1975.

Karabulut, H., Bouchon, M., Aktar, M., özalaybey, S., Schmittbuhl, J., & Bouin, M. P., "The Seismicity in the Eastern Marmara Sea after the 17 August 1999 İzmit Earthquake", *Bulletin of the Seismological Society of America*, 93(5), 2540-2551, 2003.

Kaya, T., Tank, S.B., Tuncer, M.K., Rokityansky, I.I., Tolak, E., & Savchenko, T., "Asperity Along the North Anatolian Fault Imaged by Magnetotellurics at Düzce, Turkey", *Earth, Planets and Space*, 61(7), 871-884, 2009.

King, G. C. P., Stein, R. S., & Lin, J., "Static Stress Changes and the Triggering of Earthquakes", *Bulletin of the Seismological Society of America*, 84(3), 935-953, 1994.

Lanari, R., Mora, O., Manunta, M., Mallorqui, J. J., Berardino, P., & Sansosti, E., "A Small-Baseline Approach for Investigating Deformations on Full-Resolution Differential SAR Interferograms", *IEEE Transactions on Geoscience and Remote Sensing*, 42(7), 1377-1386, 2004.

Lasserre, C., Peltzer, G., Crampé, F., Klinger, Y., Van der Woerd, J., Tapponnier, P., & Gaudemer, Y., "Coseismic Deformation of the 2001 MW= 7.8 Kokoxili Earthquake in Tibet, Measured by Synthetic Aperture Radar Interferometry", *Journal of Geophysical Research: Solid Earth*, 110(B12), 2007.

Liu, Y., & Zhang, J., "Integrating SBAS-InSAR and AT-LSTM for Time-Series Analysis and Prediction Method of Ground Subsidence in Mining Areas", *Remote Sensing, 15*(13), 3409, 2023.

Lu, Z., Dzurisin, D., & Wicks, C., "Monitoring Volcano Deformation with ALOS PALSAR Data", *Geophysical Research Letters, 34*(23), 2007.

Madsen, S. N., Zebker, H. A., & Martin, J. M., "Topographic Mapping Using Radar Interferometry: Processing Techniques", *IEEE Transactions on Geoscience and Remote Sensing, 33*(4), 915-920, 1995.

Marone, C., Scholz, C. H., & Bilham, R., "On the Mechanics of Earthquake Afterslip", *Journal of Geophysical Research: Solid Earth*, 96(B5), 8441-8452, 1991.

Massonnet, D., & Feigl, K. L., "Radar Interferometry and Its Application to Changes in the Earth's Surface", *Reviews of Geophysics*, 36(4), 441-500, 1998.

McCaffrey, R., "The Tectonic Framework of the Sumatran Subduction Zone", *Annual Review of Earth and Planetary Sciences*, 37, 345-366, 2009.

McKenzie, D. P., "Active Tectonics of the Mediterranean Region", *Geophysical Journal International, 30*(2), 109-185, 1972.

Meade, B. J., & Hager, B. H., "Block Models of Crustal Motion in Southern California Constrained by GPS Measurements", *Journal of Geophysical Research: Solid Earth*, 110(B3), 2005.

Monserrat, O., Crosetto, M., & Luzi, G., "A Review of Ground-based SAR Interferometry for Deformation Measurement", *ISPRS Journal of Photogrammetry and Remote Sensing, 93*, 40-48, 2014.

Murray, J. R., & Segall, P., "Modeling Broadscale Deformation in Northern California and Nevada from Plate Motions and Elastic Strain Accumulation", *Geophysical Research Letters*, 28(22), 4315-4318, 2001.

Nakajima, J., & Hasegawa, A., "Tomographic Imaging of Seismic Velocity Structure in and around the Onikobe Volcanic Area, Northeastern Japan: Implications for Fluid Distribution", *Journal of Volcanology and Geothermal Research*, 160(3-4), 300-312, 2007.

Nocquet, J. M., "Present-day Kinematics of the Mediterranean: A Comprehensive Overview of GPS Results", Tectonophysics, 579, 220-242, 2012.

Okada, Y., "Surface Deformation Due to Shear and Tensile Faults in a Half-Space", *Bulletin of the Seismological Society of America*, 75(4), 1135-1154, 1985.

Okay, A. I., Satır, M., Maluski, H., Siyako, M., Monie, P., Metzger, R., & Akyüz, S., "Paleo- and Neo-Tethyan Events in Northwestern Turkey: Geologic and Geochronologic Constraints", *Geological Society of America Bulletin*, 111(1), 1-22, 1999.

Okay, A. I., & Tüysüz, O., "Tethyan Sutures of Northern Turkey", *Geological Society, London, Special Publications*, 156, 475-515, 1999.

Ozener, H., Dogru, A., & Turgut, B., "Effects of Fault Geometry on Earthquake Size and Seismic Hazard in Turkey", *Geophysical Journal International, 181*(1), 518-529, 2010.

Parsons, T., Stein, R. S., Simpson, R. W., & Reasenberg, P. A., "Stress Sensitivity of

Fault Seismicity: A Comparison Between Limited-Offset Oblique and Major Strike-Slip Faults", *Journal of Geophysical Research: Solid Earth*, 104(B11), 20223-20240, 1999.

Pınar, A., Coşkun, Z., Mert, A., Kalafat, D., "Frictional Strength of North Anatolian Fault in Eastern Marmara Region", Earth Planets Space 68, 62, 2016.

Poland, M. P., Lu, Z., & Dzurisin, D., "Detailed Mapping of Volcano Deformation Using Interferometric Synthetic Aperture Radar", *Springer Science & Business Media*, 2006.

Rawlinson, N., Sambridge, M., & Hauser, J., "Multi-Scale Seismic Tomography", *Geophysical Journal International*, 179(3), 1313-1327, 2010.

Reid, H. F., "The Mechanics of the Earthquake", In The California Earthquake of April 18, 1906: Report of the State Earthquake Investigation Commission (Vol. 2, pp. 16-28). Washington, DC: Carnegie Institution of Washington, 1910.

Reilinger, R. E., Ergintav, S., Bürgmann, R., McClusky, S., Lenk, O., Barka, A., ... & Feigl, K. L., "Coseismic and Postseismic Fault Slip for the 17 August 1999, M = 7.5, İzmit, Turkey Earthquake", *Science*, 289(5484), 1519-1524, 2000.

Reilinger, R., McClusky, S., Vernant, P., Lawrence, S., Ergintav, S., Çakmak, R., ... & Kadirov, F., "GPS Constraints on Continental Deformation in the Africa-Arabia-Eurasia Continental Collision Zone and Implications for the Dynamics of Plate Interactions", *Journal of Geophysical Research: Solid Earth, 111*(B5), 2006.

Rosen, P. A., Hensley, S., Joughin, I. R., Li, F. K., Madsen, S. N., Rodríguez, E., & Goldstein, R. M., "Synthetic Aperture Radar Interferometry", *Proceedings of the IEEE*, 88(3), 333-382, 2000.

Rott, H., Scheuchl, B., Siegel, A., & Grasemann, B., "Monitoring Very Slow Slope Movements by Means of SAR Interferometry: A Case Study from a Mass Waste Above a Reservoir in the ötztal Alps, Austria", *Geomorphology, 112*(1-2), 162-170, 2009.

Savage, J. C., "A Dislocation Model of Strain Accumulation and Release at a Subduction Zone", *Journal of Geophysical Research: Solid Earth*, 88(B6), 4984-4996, 1983.

Schaff, D. P., & Richards, P. G., "Repeating Seismic Events in China", *Science*, 303(5662), 1176-1178, 2004.

Scholz, C. H., *The Mechanics of Earthquakes and Faulting*,[Edition 2], Cambridge University Press,2002.

Scholz, C. H., "Large Earthquake Triggering, Clustering, and the Synchronization of Faults", *Bulletin of the Seismological Society of America*, 100(3), 901-909, 2010.

Segall, P., Burgmann, R., & Matthews, M. V., "Time-Dependent Triggered Afterslip Following the 1989 Loma Prieta Earthquake", *Journal of Geophysical Research: Solid Earth*, 105(B3), 5615-5634, 2000.

Şengör, A. M. C., & Yılmaz, Y., 1981, "Tethyan Evolution of Turkey: A Plate Tectonic Approach", *Tectonophysics*, 75(3-4), 181-241, 1981.

Şengör, A. M. C., Görür, N., & Şaroğlu, F. "Strike-slip Faulting and Related Basin Formation in Zones of Tectonic Escape: Turkey as a Case Study, *Strike-slip deformation, basin formation, and sedimentation. Society of Economic Paleontologists and Mineralogists Special Publication, 37*, 227-264, 1985.

Şengör, A. M. C., Tüysüz, O., İmren, C., Sakınç, M., Eyidoğan, H., Görür, N., ... &

Le Pichon, X., "The North Anatolian Fault: A New Look", *Annual Review of Earth and Planetary Sciences*, 33, 37-112, 2005.

Shearer, P. M., *Introduction to Seismology*, Cambridge University Press, 1999.

Sibson, R. H., "Fault Zone Models, Heat Flow, and the Depth Distribution of Earthquakes in the Continental Crust of the United States", *Bulletin of the Seismological Society of America*, 72(1), 151-163, 1982.

Stein, R. S., Barka, A. A., & Dieterich, J. H., "Progressive Failure on the North Anatolian Fault Since 1939 by Earthquake Stress Triggering", *Geophysical Journal International*, 128(3), 594-604, 1997.

Stein, R. S., "The Role of Stress Transfer in Earthquake Occurrence", *Nature*, 402(6762), 605-609, 1999.

Tarchi, D., Rudolf, H., & Luzi, G., "SAR Interferometry for Structural Change Detection: A Case Study on a Sliding Slope", *Journal of Geophysical Research: Solid Earth, 108*(B1), 2003.

Toda, S., Stein, R. S., Reasenberg, P. A., Dieterich, J. H., & Yoshida, A., "Stress Transferred by the 1995 Mw= 6.9 Kobe, Japan, Shock: Effect on Aftershocks and Future Earthquake Probabilities", *Journal of Geophysical Research: Solid Earth*, 103(B10), 24543-24565, 1998.

Toda, S., Stein, R. S., Richards-Dinger, K., & Bozkurt, S. B., "Forecasting the Evolution of Seismicity in Southern California: Animations Built on Earthquake Stress Transfer", *Journal of Geophysical Research: Solid Earth*, 110(B5), B05S16, 2005.

Torres, R., Snoeij, P., Geudtner, D., Bibby, D., Davidson, M., Attema, E., ... & Rommen, B., "GMES Sentinel-1 Mission", *Remote Sensing of Environment*, 120,

9-24, 2012.

Waldhauser, F., & Ellsworth, W. L., "A Double-Difference Earthquake Location Algorithm: Method and Application to the Northern Hayward Fault, California", *Bulletin of the Seismological Society of America*, 90(6), 1353-1368, 2000.

Waldhauser, F., Schaff, D. P., & Pacheco, J. F., "Repeating Earthquakes in the San Andreas Fault Zone", *Science*, 303(5662), 1170-1173, 2004.

Wang, C. Y., Eken, T., Taymaz, T., & Han, L. B., "Seismic Anisotropy and Velocity Structure Beneath Turkey: Implications for Crustal Deformation and Mantle Flow", *Journal of Geophysical Research: Solid Earth*, 125(7), e2019JB019566, 2020.

Wang, H., Wright, T. J., & Parsons, B., "Source Parameters of the 2005 Mw 7.8 Kashmir Earthquake from InSAR and GPS Measurements", *Geophysical Journal International, 190*(3), 1723-1732, 2012.

Wang, R., Schurr, B., Milkereit, C., Shao, Z., & Jin, M., "An Improved Automatic Scheme for Empirical Baseline Correction of Broadband Seismic Records", *Bulletin of the Seismological Society of America*, 101(5), 2029-2044, 2011.

Wright, T. J., Fielding, E. J. & Parsons, B., "Triggered Slip: Observations of the 17 August 1999 Izmit (Turkey) Earthquake Using Radar Interferometry", *Geophysical Research Letters*, 28(6), 1079-1082, 2001.

Wright, T., "Remote Monitoring of the Earthquake Cycle Using Satellite Radar Interferometry", *Philosophical Transactions of the Royal Society of London*, Series A: Mathematical Physical and Engineering Sciences, 360, 2873-2888, 2002.

Wright, T. J., Parsons, B., & Fielding, E. J., "Measurement of Interseismic Strain Accumulation Across the North Anatolian Fault by Satellite Radar Interferometry",

Geophysical Research Letters, 31(L01607), 2004.

Wright, T. J., Parsons, B., England, P. C., & Fielding, E. J., "InSAR Observations of Low Slip Rates on the Major Faults of Western Tibet", *Science, 305*(5681), 236-239, 2004.

Yu, Y., Balz, T., Luo, H., Liao, M., & Zhang, L., "GPU Accelerated Interferometric SAR Processing for Sentinel-1 TOPS Data", *Computers & Geosciences, 129*, 12-25, 2019.

Yunjun Z., Fattahi H., and Amelung F., "Small Baseline InSAR Time Series Analysis: Unwrapping Error Correction and Noise Reduction", Computers & Geosciences, arXiv:104331 [cs.CE], 2019.

Zhao, D., Ohtani, E., & Hasegawa, A., "Deep Slab Subduction and Dehydration and Their Geodynamic Consequences: Evidence from Seismology and Mineral Physics", *Earth-Science Reviews*, 72(1-2), 61-91, 2004.